Scaffold-Based Temporomandibular Joint Cartilage Regeneration

Using Bone Marrow-Derived Mesenchymal Stem Cells

Espen Helgeland

Thesis for the degree of Philosophiae Doctor (PhD)
University of Bergen, Norway
2020

UNIVERSITY OF BERGEN

Scaffold-Based Temporomandibular Joint Cartilage Regeneration

Using Bone Marrow-Derived Mesenchymal Stem Cells

Espen Helgeland

Thesis for the degree of Philosophiae Doctor (PhD)
at the University of Bergen

Date of defense: 27.11.2020

Year: 2020

Title: Scaffold-Based Temporomandibular Joint Cartilage Regeneration

Name: Espen Helgeland

Print: Skipnes Kommunikasjon / University of Bergen

Scientific environment

The studies on which this thesis is based were undertaken between September 2016 and June 2020. The principal supervisor was Professor Annika Rosén and the co-supervisors were Professor Kamal Mustafa, Dr. Torbjørn Østvik Pedersen and Dr. Ahmad Rashad. The main work was carried out at the Department of Clinical Dentistry, Faculty of Medicine, University of Bergen (UiB), Bergen, Norway. The animal experiment was conducted at the Animal Laboratory Facility, Department of Clinical Medicine, UiB, Bergen, Norway. Imaging was conducted at the Molecular Imaging Center (MIC), UiB, Bergen, Norway. Human bone marrow aspirates were obtained at Haukeland University Hospital, Bergen, Norway. Crosslinking of scaffolds by dehydrothermal and ribose was undertaken by collaborators at The Institute of Science and Technology for Ceramics (ISTEC), Faenza RA Italy.

Acknowledgments

"*It takes a village to raise a child*". In my case, that is an understatement…

I would like to thank my team of supervisors. Annika Rosén, thank you for taking me under your wing when I expressed an interest in research. Kamal Mustafa, it has been a privilege to be a member of the Tissue Engineering Group under your leadership. Torbjørn Ø. Pedersen, you have been an inspiration and paved the way from the lab to the clinic. Ahmad Rashad, your patience, kindness, and instructive approach is the reason I managed to complete my work. I am eternally grateful! Siddharth, thank you for your friendship, for the input and for teaching me scientific writing and reasoning. Anne Christine Johannessen, I admire your knowledge and I am grateful for your contribution.

The mother of the fourth floor, Siren! Your kindness and care mean a lot to all of us. You make it a pleasure to come to work every day. Kaja, Ying, Randi and Hisham – thank you for instructing and assisting me in the lab and for being great colleagues. Stein Atle, thank you for valuable statistical assistance. And to the rest of my fourth-floor colleagues, thank you for the lively conversation and company.

To all my fellow students, current and past: Yassin, Salwa, Hassan, Mo, Samih, Ragda, Maryam, Sunita, Nageeb, Christian, Anneli, Siri, Kathrin, Dagmar, Magnus, Neha, Jannika, Shuntaro, Victoria, Elisabeth C, Elisabeth G.G., Trine Lise and Cecilie – thank you all for the great company! A special thanks to my roomies, Elisabeth S. Eriksen and Ulrik for the stimulating conversations and great friendship. An extra shoutout to my friend Øyvind for statistical assistance, for sharing the struggle with me and brightening up the darkest hours!

June, Elina, Andreas, Mona, Randi, and Marit S – thank you for facilitating, organizing, and helping me with minor and major tasks.

To my friends in the “real world” – thanks for your love, support and understanding for my absence. An extra thanks to Peter, for shifting my focus and keeping my body in shape!

To my parents, Britt and Bent, thank you for giving me every opportunity in life! Erik, Even, Eirik and Gunnar, thank you for all your support. My in-laws, Birte and Rune, thank you for your support and help with the children, making their childhood extraordinary. To my beautiful wife, Monika: You are my greatest supporter and friend! Thanks for being my rock, for holding the family together and reminding me of what is most important in life. Together with Benjamin and Filippa, you are my everything and I love you to the moon and back!

Espen Helgeland
August 2020.

List of publications

I. **Helgeland E,** Pedersen TO, Rashad A, Johannessen AC, Mustafa K, Rosén A. Angiostatin-functionalized collagen scaffolds suppress angiogenesis but do not induce chondrogenesis by mesenchymal stromal cells *in vivo*. **J Oral Sci. 2020; doi 10.2334/josnusd. 19-0327 (Online ahead of print).**

II. **Helgeland E,** Shanbhag S, Pedersen TO, Mustafa K, Rosén A. Scaffold-based temporomandibular joint tissue regeneration in experimental animal models: a systematic review. **Tissue Eng Part B Rev. 2018; 24:300-316.**

III. **Helgeland E,** Mohamed-Ahmed S, Shanbhag S, Pedersen TO, Rosén A, Mustafa K, Rashad A.
3D printed gelatin-genipin scaffolds for temporomandibular joint cartilage regeneration. *Submitted manuscript.*

IV. **Helgeland E,** Rashad A, Campodoni E, Pedersen TO, Sandri M, Rosén A, Mustafa K.
Dual-crosslinked 3D printed gelatin scaffolds with potential for temporomandibular joint cartilage regeneration. *Submitted manuscript.*

List of abbreviations

ACAN	Aggrecan
ACI	Autologous chondrocyte implantation
AGEs	Advanced glycosylated end products
ALP	Alkaline phosphatase
αMEM	Alpha minimum essential medium
ANOVA	Analysis of variance
ARRIVE	Animal Research: Reporting *In Vivo* Experiments
BMSC	Bone marrow-derived stem cells
BMP	Bone morphogenetic protein
BSA	Bovine serum albumin
BTE	Bone tissue engineering
CAD	Computer-aided designed
CAM	Computer-aided manufacturing
CC	Chondrocytes
CD	Cluster of differentiation
COL	Collagen
CT	Computed tomography
CTE	Cartilage tissue engineering
CTGF	Connective tissue growth factor

DAPI	4′,6-Diamidino-2-phenylindole dihydrochloride
DHT	Dehydrothermal
FDA	Food and Drug Administration
FDM	Fused deposition modelling
FU	Fluorescence units
GADPH	Glutaraldehyde 3-phosphate dehydrogenase
GAG	Glycosaminoglycans
GFs	Growth factors
GMP	Good manufacturing practice
GRAS	Generally Regarded As Safe
GTA	Glutaraldehyde
hBMSC	Human bone marrow-derived stem cells
H&E	Hematoxylin and eosin
ID	Internal derangements
ISCT	The International Society for Cellular Therapy
IVD	Intervertebral disc
μCT	Micro computed tomography
MMP	Matrix metalloproteinase
MRI	Magnetic resonance imaging
MSC	Mesenchymal stem cells

MTC	Masson's trichrome
OA	Osteoarthritis
PBS	Phosphate buffered saline
PCL	Polycaprolactone
PECAM1	Platelet endothelial cell adhesion molecule 1
PFA	Paraformaldehyde
PGA	Poly glycolic acid
PICO	Population, Intervention, Comparison, Outcome
PLA	Poly lactide acid
PLGA	Poly lactic-co-glycolic acid
PRISMA	Preferred Reporting Items for Systematic reviews and Meta-Analysis
PTFE	Polytetrafluoroethylene
rBMSC	Rat bone marrow-derived stem cells
RCT	Randomized controlled trial
RGD	Arginine-Glycine-Aspartate
RPM	Rotations per minute
RT-qPCR	Real Time – Quantitative Polymerase Chain Reaction
SOX	SRY-related high-mobility group-box gene
SEM	Scanning electron microscope
SYRCLE	Systematic Review Center for Laboratory Animal Experimentation

3D	Three-dimensional
TE	Tissue engineering
TGF	Transforming growth factor
TMD	Temporomandibular disorders
TMJ	Temporomandibular joint
VEGF	Vascular endothelial growth factor

List of tables

List of figures

Abstract

Reconstruction of lost or damaged cartilaginous structures of the temporomandibular joint (TMJ) presents a clinical challenge and current treatment options are limited. The potential for repair is poor, because cartilage is avascular and degenerated structures are traditionally surgically removed, to improve function and reduce the level of pain. The studies in this thesis were undertaken to explore the possibility for regeneration of TMJ cartilage by means of tissue engineering (TE). The main objective of this thesis was to develop a regenerative approach for degenerated TMJ cartilage, combining bone marrow-derived stem cells (BMSC) with a natural polymer scaffold.

Study I is a pilot study, investigating the *in vivo* effect of the angiogenesis inhibitor, angiostatin, on BMSC seeded collagen scaffolds. After subcutaneous implantation in rats for two weeks, angiostatin downregulated the levels of inflammatory and angiogenic gene markers and decreased vessel formation in the constructs. However, histological examination disclosed that this strategy alone did not induce cartilage formation.

Based on the above findings, and the observed lack of established methods for TMJ cartilage TE, a systematic literature review (Study II) was undertaken to assess the *in vivo* evidence for TMJ TE. In total, the search yielded 30 studies of ectopic and orthotopic models investigating regeneration of the TMJ disc, condyle, and synovial membrane, in five different species. Overall, the use of BMSC and natural polymer scaffolds was most frequently reported. With respect to regenerative potential, differentiated stem cells were reported to be superior to undifferentiated cells.

The systematic review disclosed the beneficial effects of BMSC combined with scaffolds of natural polymers, such as collagen and gelatin. With respect to TMJ regeneration by TE, the preferred scaffolding material for investigation was gelatin, because of its biocompatibility, superior hydrogel-forming properties and lower costs in comparison with collagen. In Study III, a gelatin hydrogel was 3D printed, crosslinked with genipin and characterized in terms of swelling, stability, degradation,

mechanical properties and cytotoxicity. The chondrogenic differentiation potential of human BMSC (hBMSC) seeded on the developed scaffolds was compared with that of hBMSC in traditional pellet or novel spheroid cultures. Genipin successfully prevented rapid degradation of the scaffolds, which supported cell attachment and proliferation without adverse cytotoxic effects. Scaffolds seeded with hBMSC followed the same trend in upregulation of chondrogenic gene markers, but at lower levels than for pellet and spheroid cultures. It was noteworthy that the hypertrophy marker collagen type 10 was downregulated in hBMSC on scaffolds, in comparison with spheroids and cell pellets. The chondrogenic differentiation of hBMSC on the 3D printed scaffolds was confirmed by Alcian blue and immunofluorescence staining.

In Study IV, dehydrothermal (DHT) treatment was compared to ribose and the dual crosslinking with both DHT and ribose. The scaffolds were characterized with respect to swelling, stability, enzymatic degradation, and degree of crosslinking. Cell-seeding efficiency, attachment, proliferation, glycosaminoglycan (GAG) formation and differentiation of rat BMSC were compared between the groups. While the dual crosslinking resulted in the highest degree of crosslinking, stability, enzymatic resistance, mechanical properties, and proliferation, DHT had the highest cell seeding efficiency and viability. Ribose had the highest swelling capacity, but the lowest stability, enzymatic degradation, mechanical properties, cell seeding density and chondrogenic differentiation potential. However, no differences were observed with respect to GAG formation.

In summary, inhibition of vascularization alone was not enough to stimulate chondrogenesis in TE constructs (Study I), indicating the need for alternative approaches. The current preclinical evidence clearly demonstrates the beneficial effects of using natural polymer scaffolds combined with MSC for TMJ TE (Study II). Gelatin, one such polymer, was found to be suitable for fabrication of 3D printed scaffolds, which support the proliferation and chondrogenic differentiation of hBMSC (Study III). Finally, dual crosslinking of 3D printed gelatin scaffolds with DHT and ribose enhanced the degree of crosslinking, mechanical properties, enzymatic resistance and stability (Study IV).

Contents

1. Introduction

1.1. Clinical challenge

Temporomandibular disorders (TMD) are a subgroup of multifactorial craniofacial pain conditions, clinically manifest in the musculoskeletal structures of the head and neck [1]. The prevalence in the population is 3-12 % [2, 3] and reportedly more frequent (2-9 times) in women than men [1, 4]. The temporomandibular joint (TMJ) is a bilateral synovial joint (Figure 1) with both sliding- and hinge movements, of great importance for daily activities such as speaking and chewing [5]. It connects the mandible to the temporal fossa and is separated by a disc [6]. The disc provides lubrication for smooth movements, in addition to absorbing loads during mastication, in many ways analogous to the meniscus in the knee. The disc is composed of fibrocartilage, in which the main component is collagen type 1 (COL1), with a biconcave shape to fit the mandibular condyle [7]. The mandibular condyle has a superficial layer of fibrocartilage, but with additional zones of COL2 dominated hyaline cartilage-like architecture, with proliferative, mature and hypertrophic zones, towards the underlying bone [8]. In a healthy situation, the disc follows the condylar movements.

Displacement of the TMJ disc, most commonly anteriorly, which interferes with smooth joint movements, is called internal derangement (ID) [9]. The displacement can be reversible, associated with painful clicking, or constitute a sustained mechanical obstacle, *i.e.* chronic closed lock [10]. ID is considered to be a TMD and is often conjugated with osteoarthritis (OA), but it is unclear whether they are causative events, or if one precedes the other [11]. Nevertheless, the trauma to the disc can over time lead to disc thinning and perforations, which are considered to be the first of a series of degenerative changes [12, 13].

Degenerative joint diseases constitute a significant global health problem [14], expected to increase as the population ages [15]. OA is the most prevalent joint disease [16] and leads to breakdown of cartilaginous and bony structures, resulting in impaired

function and quality of life [17]. Degenerative changes are most frequently observed in load-bearing joints, *e.g.* knee and spine, but are also a frequent finding in the TMJ [18]. Risk factors for OA development include joint injury, obesity, aging and heredity. However, the molecular mechanisms underlying initiation and progression of OA in general [19] and TMJ OA specifically [20], are elusive and poorly understood. Moreover, the lack of blood and nerve supply within cartilaginous tissues contributes to low repair potential and lesion progression [21].

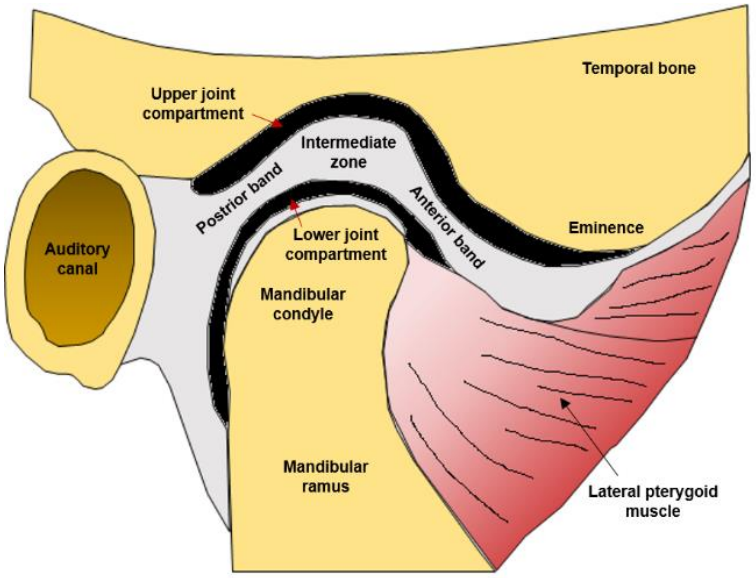

Figure 1. The temporomandibular joint and associated structures.

Most TMD are treated with non- or minimally invasive approaches, such as physical therapy, occlusal splints, pharmacological agents, intra-articular injections, arthrocentesis and arthroscopy [1]. However, approximately 5-10 % of patients who seek treatment for TMD do not respond to conservative treatment [22] and fewer than 1 % are candidates for surgical interventions [23]. In some cases, the diseased TMJ disc is surgically removed (discectomy) [24] and postoperatively improved function and decreased pain are reported [25], but to prevent further degeneration, and in severe cases ankylosis of the mandible to the temporal bone, a interpositional disc replacement material is often recommended [26].

In the 1970's and 80's alloplastic silicone-rubber and polytetrafluoroethylene (PTFE) implants were used, with catastrophic long-term clinical results [27]: material fragmentation and foreign body reactions with giant cell infiltrates due to biomechanical overloading were observed in the TMJ [27]. Since then, autologous grafts of dermis and/or fat, or temporal muscle are preferred [26]. These provide temporary replacements to cover the osteotomized bone surfaces during healing, but require more invasive surgery with associated donor site morbidity [28]. Insertion of a total joint prosthesis, completely replacing the condyle and fossa component with an alloplastic device, is a biomechanical solution reserved for a small group of end-stage TMD patients [29]. Despite improved long-term success of the devices, the complexity of the physiological and biomechanical environment affects the longevity [29]. Hence, revisions during the patient's lifetime are likely, with associated increased costs and patient-burden [30].

Thus, there is currently a gap in treatment options available for repair of TMJ structures damaged by degenerative TMJ changes [20].

1.2. Cartilage Tissue Engineering (CTE)

Historically, fibrocartilage injuries have been treated by removal of the affected structures [31], *e.g.* knee meniscectomy [32], or TMJ discectomy [25]. While this may increase the function and decrease the symptoms, it does not repair and restore the lost or damaged functional structures. This has led to a paradigm shift, towards regenerative strategies. Pioneering work by Langer and Vacanti, using three dimensional (3D) porous scaffolds to culture cells [33] has evolved into what is today referred to as tissue engineering (TE). The concept includes the use of cells from the patient, often combined with biomaterial(s) serving as a template/scaffold for regeneration and neotissue formation [34]. It has been proposed that cartilage, a homogenous, avascular tissue containing few cell types, would be an ideal candidate for CTE [35].

1.2.1. Cell types

Chondrocytes

Chondrocytes (CC), which comprise the cellular component of cartilage, are mature cells with the inherent ability to secrete cartilaginous matrix. They have therefore been widely used in attempts at cartilage regeneration [36]. An early study and one of the most renowned, is from Vacanti's group, who seeded bovine CC onto polyglycolic acid (PGA) scaffold with the anatomical shape of a human ear [37]. After 12 weeks of subcutaneous implantation in athymic mice, the construct successfully formed neocartilage. In orthopedics, autologous chondrocyte implantation (ACI), *i.e.* harvesting and expansion of CC before re-transplantation [38], and microfracture marrow stimulation, *i.e.* perforating the site of injury to recruit progenitor cells for repair, are established clinical methods with varied success in replicating native tissue [35].

Despite the established clinical application of ACI in orthopedics [39], there are few such studies on the TMJ. An exception is a recent study reporting injection of autologous nasal septum-derived CC for regeneration of condylar resorption after orthognathic surgery [40]. Six months after injection of 10 million cells per TMJ, computed tomography (CT) images revealed regeneration of cartilaginous and bony defects. One year later, CT images revealed cortical and subcortical bone formation, partially reconstructing the original anatomy. Albeit a single case, this study presents a concept for cell-based condylar regenerative treatment, preventing or delaying the need for an alloplastic total joint prosthesis [40].

CC have been harvested from numerous sites for various CTE applications, for example hyaline cartilage CC from costal ribs [41, 42], articular joints [41] and nose [43], elastic cartilage from the ear [44] and fibrocartilage CC harvested from the TMJ condyle [45] and intervertebral disc (IVD) annulus fibrosis [46]. Although CC are considered to be immune privileged, the potential use of allogenic CC is still limited by donor availability and the risk of disease transmission [36]. Harvesting of CC requires secondary surgery, with associated donor site morbidity and risk of complications [35]. For example, apart from infections, OA development has been

reported even from small biopsies from non-weight bearing joints [21]. Furthermore, *in vitro* expansion for adequate cell numbers has demonstrated limited life span, loss of phenotype through dedifferentiation and senescence of the CC [47] with decreased matrix secretion [36], making them less than ideal candidates for cell-based CTE.

Mesenchymal stem cells

The limitations of CC have led to investigation of alternative cell sources. The potential of mesenchymal stem cells (MSC) has been widely investigated for several applications after their discovery by Friedstein et al. in 1968 [48]. MSC are multipotent cells with the ability to differentiate into cells of mesodermal origin, *e.g.* bone, fat, muscle, tendon and cartilage [49]. They were first isolated from bone marrow (BMSC), and consequently most extensively investigated [49]. However, the fraction of MSC is limited to 0.001% - 0.01% of the total number of bone marrow nucleated cells [50]. This requires massive *in vitro* expansion to achieve adequate cell numbers for clinical use. In contrast to CC, MSC can be expanded with lower risk of losing their phenotype [38]. Furthermore, MSC need to be characterized to ensure that they meet the minimal criteria defined by The International Society for Cellular Therapy (ISCT) *i.e.* plastic adherence, tri-lineage differentiation capacity and cluster of differentiation (CD) and human leukocyte antigen DR isotype (HLA-DR) surface marker expression ($CD73^+$, $CD90^+$, $CD105^+$, $CD34^-$, $CD45^-$, $HLA\text{-}DR^-$) [51]. These characteristics enable MSC to be distinguished from hematopoietic cells, but may still not ensure homogenous MSC populations [36]. Due to the invasiveness of bone marrow aspirations, alternative sources have been explored, *e.g.* adipose tissue, synovial tissue, dental pulp and others [52]. ASC are more abundant and easily accessed than BMSC, but with reportedly inferior chondrogenic differentiation potential [36, 53, 54].

Regardless of the source, individual donor variability of MSC is a challenge with respect to proliferation and differentiation capacity [54], which may require tuning of cell density on a donor-by-donor basis for successful stable neotissue formation [55]. Furthermore, the time and cost of individual monolayer expansion in a Good Manufacturing Practice (GMP) facility to obtain the required cell numbers may limit their applications [36].

MSC contribute to repair and regeneration by differentiating into specific cell types, and/or secreting soluble bioactive molecules (*e.g.* growth factors [GFs], cytokines and chemokines). It is proposed that these trophic or paracrine effects which stimulate host progenitor cells and modulate immune cells [56], are the main effect of MSC in regeneration and the reason Caplan argues that MSC should be referred to as 'medicinal signaling cells' [57]. The paracrine effects of MSC have recently been reported clinically [58]. Allogenic MSC were co-cultured with autologous articular cartilage-derived cells (including pericellular matrix) in a 90:10 or 80:20 ratio for treatment of isolated articular defects in the knee of 10 young patients (mean 26 ± 5 years) [58]. The cells were mixed with fibrin glue and implanted without adverse effects, proving the safe clinical use of allogenic MSC. The defects healed and were close to 'normal tissue' in six patients and 'nearly normal' in three of the nine patients approving a second-look arthroscopy at 12-month follow-up. No allogenic cells were present in the repair tissue after 1 year and no immune responses were observed. The authors proposed that the MSC served as a "drug-store" [59], providing a regenerative microenvironment and regulating the immune response *in vivo*.

Chondrogenic differentiation of MSC

Chondrogenic differentiation is regulated by several signaling pathways [60]. Embryonically, MSC condensations result in SRY-related high-mobility group-box gene 9 (SOX9) expression which is considered a key regulator of chondrogenesis [61]. Expression of transcription factors SOX5, SOX6 together with SOX9 are seen in immature CC, together with the proteins COL2 and aggrecan (ACAN), all considered markers for CC differentiation [60]. SOX9 is expressed in healthy cartilage throughout life but repressed in hypertrophic CC [62]. Heterozygous mutations of this gene lead to severe skeletal malformations, *e.g.* campomelic dysplasia, dwarfism, cleft palate and can be potentially lethal when affecting the airways [62, 63]. SOX9 also regulates other chondrogenic genes, *e.g.* ACAN [64] and COL2 [65]. ACAN is a major structural core protein in cartilage and categorized as a proteoglycan [66]. With connected glycosaminoglycans (GAG) it forms hydrated gels, considered crucial for the load-bearing capacity of cartilage [66].

A standard method for *in vitro* chondrogenic differentiation is by means of MSC aggregated in pellets and cultured in chondrogenic defined medium [67, 68]. The high density and close proximity stimulate communications through diffusible signals and cell-cell interactions, and aims to mimic the embryological mesenchymal condensations [60, 67]. The medium is typically supplemented with dexamethasone, ascorbate-2-phosphate, insulin, selenious acid, transferrin, sodium pyruvate and transforming growth factor beta [69]. After two to three weeks of pellet culture, ECM with primary cartilage-specific molecules *e.g.* COL2 and ACAN, is expected to be present [69]. However, nutrient supply to the core of the pellet is limited, resulting in necrosis [70].

While pellet cultures have been used for chondrogenic differentiation for decades, more recently, aggregated cell cultures of MSC have attracted interest for several applications [71]. To overcome the limitations of monolayer cultures such as altered immune properties and low survival rate post-transplantation, smaller sized aggregates, *i.e.* cell spheres, have been investigated [71, 72]. Enhanced anti-inflammatory and regenerative effects, in addition to enhanced cell survival after transplantation and differentiation potential have been described [73]. Cell spheres can be formed by different techniques *e.g.* self-assembling in ultra-low attachment wells, hanging drop or microwell plates [73]. These methods are common for pluripotent stem cells and embryoid body formation, as the 3D culture replicates the intercellular interactions of embryonic cells [74]. While the self-assembly process and hanging drop technique are easy to implement, they result in poor standardization with respect to size, viability and efficiency [75]. However, microwell plates have emerged as a high-throughput method to control size and preserve viability [68, 76, 77].

Hypertrophy, a challenge of differentiated MSC, is associated with increased expression of COL10, alkaline phosphatase (ALP), matrix metalloproteinase 13 (MMP13) and vascular endothelial growth factor (VEGF), with decreased levels of chondrogenic differentiation markers [36]. This leads to invasion of osteogenic and endothelial cells replacing the cartilage template by bone through endochondral ossification [38, 60], an undesired outcome for engineered cartilage. Several strategies

to minimize this limitation have been proposed [38]. Co-culture of MSC and CC have been reported as promising [78], but would not obviate the need for CC harvesting. Alternative sources of MSC have been investigated, and synovium-derived MSC have displayed decreased hypertrophy potential, compared to BMSC and ASC [79]. Others have sought to suppress angiogenesis by using strategies intended to inhibit vascularity of either cells [80] or scaffold [81].

1.2.2. Scaffolds

Traditional two-dimensional cell cultures do not replicate the various 3D microenvironments in the human body [82]. Scaffold-free approaches, *i.e.* self-assembly and self-organization strategies, are 3D cultures using high cell densities to stimulate matrix secretion and lead to mature implants which integrate more easily [83]. However, this strategy is limited to smaller defects and is less applicable to more extensive replacements and defects. Hence, the current project focused on scaffold-based strategies. The goals of biomaterial scaffolds are to simulate the native *in vivo* ECM for implanted cells, stimulating proliferation and differentiation and to recruit endogenous progenitor cells to induce regeneration. Irrespective of the targeted tissue, a scaffold must possess the following properties [82] – (a) the material(s) should replicate the native tissue geometry (*i.e.* size and shape) to fill and replace the desired defect(s), (b) it should be biodegradable at a rate matching the formation of new tissue, and (c) the degradation products should be removed without provoking inflammatory host responses [84]. To fulfill all these requirements is challenging.

A wide range of biomaterials has been investigated for CTE. Broadly, they can be divided into synthetic and natural polymers, or hybrid mixtures of the two [85]. Synthetic polymers can be tailored with respect to their mechanical properties and degradation rate [86], important features for cartilage regeneration. Polycaprolactone (PCL) with microsphere-incorporated GFs have been used without implanted cells for TMJ disc defect regeneration [87] and polylactide (PLA) has been investigated for TMJ disc implants [88]. However, in addition to acidic degradation products, synthetic

polymers tend to have hydrophobic surface properties, which can prevent cell adhesion and protein absorption [86].

Natural polymers such as collagen, gelatin, fibrin, chitosan and silk are widely used [82]. The natural origin mimics the native ECM and are biocompatible and biodegradable. However, limitations are weak mechanical properties and *in vivo* stability. Hybrid composite materials of natural and synthetic polymers have been developed to overcome the limitations of single polymer materials. The hydrophobicity of synthetic polymers can be modified by incorporating functional ligands from natural materials. Weak mechanical properties can be enhanced by incorporating synthetic polymers [82] or by using different methods to cure the material, *e.g.* crosslinking.

Collagen as scaffold biomaterial

Collagen is the most abundant protein in mammals, present in several tissues, such as cartilage, bone and tendons, and constitutes about 30 % of the body's total protein content [89, 90]. The collagen molecule forms a triple helix of three α-chains of approximately 1000 amino acids each, with a molecular weight of 100 kDa [89]. At least 29 different types of collagen have been identified in vertebrates and invertebrates, with differences in sequence, structure and function [89] – all with the primary function of structurally stabilizing tissues and organs.

Collagen contains the amino acid ligands of Arginine-Glycine-Aspartate (RGD sequences), which are important binding motifs for cell attachment, able to initiate an intracellular signaling pathway, which stimulates cellular proliferation and maintenance of phenotype [91]. Because of its abundancy, biocompatibility and biodegradability, COL1 is a major fibrillar type most commonly used as scaffold biomaterial for CTE [91]. While COL1 is the main constituent in fibrocartilage [7], COL2 is the major component of articular hyaline cartilage and for this reason has been proposed to support chondrogenic stimulation [91]. However, COL2 has reportedly arthritogenic potential and has failed to gain approval by several health agencies, thus limiting clinical application [91].

Gelatin as scaffold biomaterial

Gelatin has been used for decades in food, cosmetics and pharmaceuticals [92] and is recognized as Generally Regarded As Safe (GRAS) by the United States Food and Drug Administration (FDA) [93]. Gelatin is a heterogeneous mixture of peptides [89] of natural origin derived from chemical hydrolysis of collagen [94]. The triple helical structure of collagen can be denatured by either acidic (type A) or alkaline (type B) hydrolysis [92], breaking up the tertiary structure [94]. The most common source of gelatin is porcine and bovine skin for type A and type B, respectively [95]. The alkaline treatment leads to a higher carboxylic acid content in type B [90]. Gelatin has several advantages for biomedical applications: low costs, high hydrophilicity, biocompatibility and biodegradability [96]. The abundant RGD sequences ensure cell attachment without compromising the cell phenotypes. However, gelatin derived from pigskin is the only source containing aspartic acid, which is an essential amino acid in the RGD sequence [97].

Collagen and gelatin can form both porous scaffolds and hydrogels for 3D printing [90]. However, they have poor mechanical properties and *in vivo* stability [94, 98]. These properties can be improved by crosslinking, with plentiful options due to the many functional groups accessible for chemical or physical modification [92].

Scaffold crosslinking

Crosslinking induces links between the polymer chains, forming 3D networks. The process may be generally described as enzymatic, chemical or physical , depending on the methods used to tailor the mechanical, biological and degradation properties of the material [99]. For TE applications, the cytotoxicity of the material and crosslinking agents are important factors, as cellular responses can be influenced by both the crosslinking agents and the soluble products that may leach out.

Enzymatic crosslinking includes microbial transglutaminase (mTGase), horseradish peroxidase and hydrogen peroxide. These methods provide mild reaction conditions, high efficiency and good cytocompatibility [99]. For TE applications, mTG is one of the most frequently applied methods of crosslinking collagen and gelatin scaffolds [99, 100].

Chemical crosslinking by glutaraldehyde (GTA) is widely used due to the low cost and high efficacy [99]. In addition to polymer scaffolds it is used to crosslink artificial cardiovascular prostheses from decellularized ECM (allogenic and xenogenic) [101]. However, calcification of the constructs are reported [101], an undesired outcome for both vascular prostheses and CTE. Moreover, the aldehyde groups are cytotoxic and can potentially cause severe inflammation during degradation.

Genipin is a natural, chemical crosslinker extracted by hydrolysis from the fruit *Gardenia jasminoides* [99]. In addition to promising biological properties [102], it has been shown to be an efficient crosslinker [99]. It forms dark blue pigments within the matrix by bridging lysine or hydroxylysine of the polypeptide chains [103] of various natural polymers, *e.g.* chitosan, collagen and fibrinogen [104-106]. However, the high costs may limit mass production [99]. In contrast, sugar, *e.g.* ribose or glucose, is an inexpensive and accessible alternative for chemical crosslinking. The crosslinking efficiency of ribose is reported to be higher than for glucose, but the reactions are similar [107]. The crosslinking is initiated by the Maillard reaction which generates advanced glycosylated end products (AGEs) [55] leading to glycation of free amino acids and proteins, improving mechanical strength and resistance to degradation [56, 57].

Dehydrothermal (DHT) treatment is a physical crosslinking method that combines vacuum and high temperature (>100 °C) over time. Water molecules are removed and two complementary functional groups are bonded through esterification or amide formation, preventing the fibers from sliding past each other under stress [108]. This method is free from chemical reagents and has been reported to be superior to chemical genipin crosslinking for cartilage regeneration [108]. In addition to stabilization, DHT treatment also sterilizes the material, increases cellular activity and decreases the immunogenic response [109].

3D printed scaffolds

Fabrication methods for scaffolds have evolved over time. Traditionally, porous scaffolds have been fabricated by ‘moulding’ followed by freeze-drying, ‘solvent casting and particular leaching’ or ‘gas foaming’ [82]. Freeze-drying of a frozen

polymer solution removes ice crystals under vacuum directly from the solid phase to gas – resulting in a dry, porous structure. Solvent casting and particular leaching use porogens in a polymer-solvent solution that are dissolved after moulding. Gas foaming creates pores by gas (*e.g.* carbon dioxide) bubbles of a solid polymer, eliminating the need for solvents [110]. While these methods are easy and inexpensive, they are limited by the control of pore size, interconnectivity, geometry and reproducibility [110].

Advances within rapid prototyping and additive manufacturing have emerged, known as 3D printing. In this process, scaffolds are created by means of a computer-aided design (CAD) model which can be obtained from medical imaging methods, *e.g.* CT or magnetic resonance imaging (MRI). The CAD object is sliced in cross-sectional layers of preferred thickness, depending on the nozzle size used to print the project. The CAD file instructs the printer head in movements in x, y and z-directions and the software allows adjustments of parameters, *e.g.* pressure, speed and temperature, depending on the material properties. This facilitates controlled pore size and customized geometry to fit the defect and permits creation of regional variances reminiscent of the native structure [111].

Different 3D printing methods have been used for scaffold fabrication. A common method today is extrusion-based printing that utilizes pneumatic pressure to extrude a soft polymer through the nozzle of the printing head, to the platform, and is compatible with both synthetic and natural polymers.

1.2.3. Preclinical TMJ models

To test the efficacy of experimental therapy, preclinical animal models are applied in both small and large animal models. Preclinical testing is important for translational research and often a requirement for regulatory health agencies before initiation of clinical trials [112]. Small animals like mice, rats and rabbits are often used for proof of principle studies [112] due to their low cost, easy handling and housing conditions compared to larger animals [113]. Mice and rats are commonly used for degenerative joint disease models, which can be either chemically induced (for pain), surgically induced (to mimic degenerative defects) or mechanically induced (to investigate

structure and function) [114]. Also widely used are ectopic models like subcutaneous implantation, and immunocompromised animals are used for xenograft implantation(s). The small size of rodent's TMJ limits their use for orthotopic models. It is possible however, to conduct experimental TMJ surgery in rabbits [87, 88]. Larger animals, like dogs, sheep, goats, farm pigs and minipigs, are more costly, but more closely resemble clinical conditions with respect to anatomy and function and can better predict the therapeutic efficacy [114]. However, animal models will never fully replicate the disease pathogenesis, morphology, forces, and function of a clinical setting.

2. Rationale

Degenerative joint diseases are prevalent and expected to increase as the population ages. The poor potential of cartilage for self-repair, often results in progressive lesions with associated disability. For patients suffering from degenerative TMJ diseases, there is a gap between early, conservative, and minimally invasive treatment options and end-stage surgical treatments with discectomy or total joint prostheses. Previous reports of failures from alloplastic TMJ disc implants and incomplete preclinical investigations, highlight the importance of thorough *in vitro* and *in vivo* testing. Extensive research has been conducted into regenerating lost and damaged cartilaginous structures. Within orthopedics, articular hyaline cartilage and knee meniscus fibrocartilage have been investigated more extensively than TMJ structures. CC are often used due to their inherent ability to secrete cartilaginous matrix – but clinical applicability is limited because of the invasive harvesting procedure and donor site morbidity. BMSC have chondrogenic differentiation potential and the harvesting is less invasive. Although promising results have been reported for several applications, hypertrophic transformation is an obstacle frequently reported when BMSC are differentiated into the chondrogenic lineage. Several scaffold biomaterials have been used, but the results from the alloplastic disc implants highlight the importance of developing optimized, biocompatible clinical implants. Natural polymers are biodegradable and biocompatible, and some can form 3D printable hydrogels. Additive manufacturing allows for customized geometry and controlled porosity, compared to traditional scaffold fabrication methods. Collagen is an obvious candidate, considering the composition of fibrocartilage. However, gelatin has many of the same advantages at a lower cost. The disadvantages of using natural polymers are their weak mechanical properties and thermo-instability, which necessitates crosslinking. Traditional crosslinkers, *e.g.* GTA and formaldehyde, are reported to be cytotoxic. Therefore, alternative methods need to be explored.

In this context, the present thesis describes research into *in vivo* and *in vitro* methods of TMJ cartilage regeneration, based on a combination of natural polymer scaffolds and BMSC.

3. Aims

The main objective of this thesis was to develop a regenerative approach for degenerated TMJ cartilage, combining BMSC with a natural polymer scaffold. The specific aims for each study were as follows:

Study I

To investigate the effect of angiostatin on inhibiting angiogenesis in collagen scaffolds loaded with rat BMSC *in vivo* as a strategy for cartilage regeneration.

Study II

To conduct a systematic review of the literature, for preclinical evidence of scaffold-based TE approaches for cartilage regeneration.

Study III

To develop and characterize (mechanically and biologically) 3D printed gelatin scaffolds, crosslinked with genipin for cartilage regeneration.

Study IV

To evaluate different crosslinking methods for 3D printed gelatin scaffolds developed for cartilage regeneration.

4. Materials and methods

4.1. Thesis design

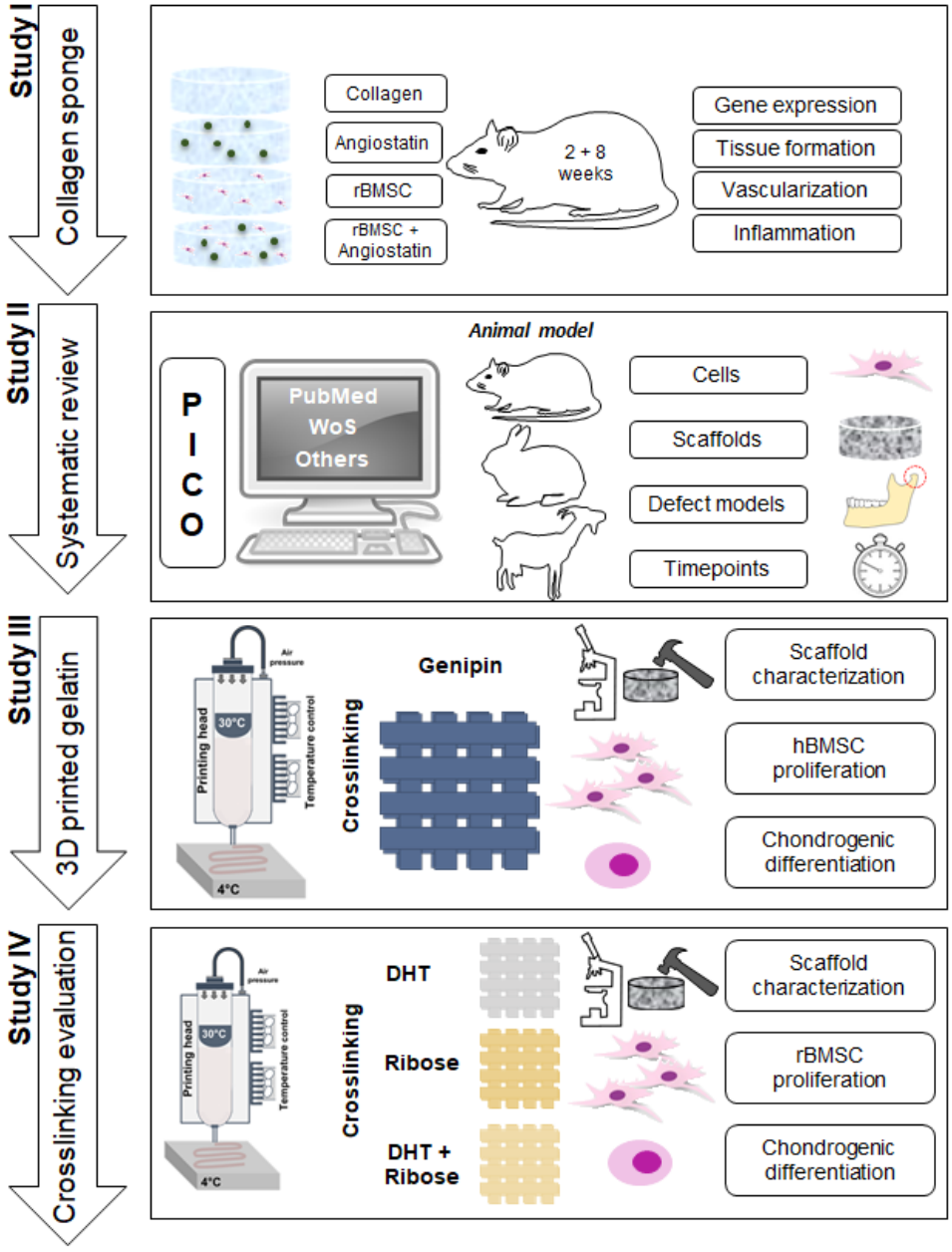

Figure 2. Schematic summary of the study designs used in the thesis.

4.2. Materials

Table 1. Materials and equipment used in the thesis

Description	Supplier	Study
	Materials	
Collagen I scaffolds	Optimaix 3D, Matricel GmbH, Herzogenrath, Germany	I
Angiostatin	Merck Millipore, MA, USA	I
Gelatin Type A	Sigma-Aldrich, MO, USA	III, IV
Genipin	Wako Chemicals GmbH, Neuss, Germany	III
Ethanol	Sigma-Aldrich, MO, USA	III
Alpha minimum essential medium	αMEM, Gibco, Thermo Fischer Scientific, MA, USA	I, III, IV
Heparin	Leo Pharma A/S, Ballerup, Denmark	III
Bovine serum albumin	Sigma-Aldrich, MO, USA	III
Cell culture flasks	NUNC A/S, Roskilde, Denmark	I, III, IV
Penicillin/streptomycin	HyClone, GE Healthcare, IL, USA	I, III, IV
FBS	HyClone, GE Healthcare, IL, USA	I, III, IV
Chondrogenic medium	StemPro, Thermo Fischer Scientific, MA, USA	III, IV
Adipogenic medium	Stem Pro Adipogenesis Differentiation Kit (Gibco, Thermo Fischer Scientific)	III
PBS	Invitrogen, Thermo Fischer Scientific, MA, USA	I, III, IV
Triton-X (0.1% in PBS)	Sigma-Aldrich, MO, USA	III, IV
PicoGreen	Quant-IT, Thermo Fischer Scientific, MA, USA	III, IV
DAPI	Sigma-Aldrich, MO, USA	I, III, IV
RNAlater	Invitrogen, Thermo Fischer Scientific, MA, USA	I
RNA extraction kit	Maxwell, Promega, WI, USA	I, III, IV
cDNA kit	Applied Biosystems, CA, USA	I, III, IV
RT-qPCR master mix	TaqMan Fast Universal, Applied Biosystems, CA, USA	I, III, IV
Optimal Cutting Temperature compound for cryosection embedding	O.C.T., Tissue-Tek, Sakura Finetek, Tokyo, Japan.	I
alamarBlue	Invitrogen, Thermo Fischer Scientific	III, IV

Live/dead assay	Invitrogen, Thermo Fischer Scientific	III, IV
Blyscan sGAG assay	Biocolor, United Kingdom	IV
Mounting medium	Prolong Gold Antifade, Invitrogen, Thermo Fischer Scientific, MA, USA	I, III, IV
Equipment		
Cell analyzer	BD LSRFortessa, BD Biosciences, CA, USA	III
Thermal cycler system	SimpliAmp, Applied Biosystems, CA, USA	I, III, IV
RT-qPCR system	StepOne System, Applied Biosystems, CA, USA	I, III, IV
Aggrewell400	STEMCELL Technologies, Vancouver, Canada	IV
Glass slides	Superfrost Plus and Polysine, Thermo Fischer Scientific, MA, USA	I, III, IV
Countess cell counter	Invitrogen, Thermo Fischer Scientific, MA, USA	I, III, IV
Internal reflection fluorescence microscope	TIRF, Nikon, Eclipse 80i, Tokyo, Japan	I, III, IV
Stereomicroscope	Leica M205 C, Leica Microsystems GmbH, Wetzlar, Germany	III, IV
Inverted light microscope	Nikon Eclipse TS100, Tokyo, Japan	I, III, IV
Confocal microscope	Dragonfly 505, Andor Technology Ltd., Belfast, Great Britain	III, IV
Micro-CT	SkyScan 1172, Bruker, Kontich, Belgium	III, IV
Sonicator	Sonopuls HD2200, Bandelin, Berlin, Germany	I, III, IV
Microplate reader I	FLUOstar OPTIMA, BMG Labtech, Ortenberg, Germany	III, IV
Microplate reader II	Varioskan LUX multimode	III, IV
Sputter coater	Q150TES, Quorum, Italy	III, IV
Scanning electron microscope	JEOL JSM-7400F, Tokyo, Japan	III, IV
Scanning electron microscope	Phenom XL Desktop SEM, Thermo Fischer Scientific, MA, USA	III
Freeze-dryer	Labonco Corporation, MO, USA	III, IV
Microtome	Leica, Wetzlar, Germany	I, III, IV
Cryomicrotome	Leica CM 3050S, Wetzlar, Germany	I

3D-printer	3D-Bioplotter, EnvisionTEC Gmbh, Gladbeck, Germany	III, IV
Syringe barrels	30cc, Optimum, Nordson, OH, USA	III, IV
Printing nozzles	400 µm, Optimum, Nordson, OH, USA	III, IV

4.3. The *in vivo* effect of angiostatin functionalized scaffolds (Study I)

4.3.1 Preparation of functionlaized collagen scaffolds

Cells were isolated from the femur of Lewis rats in accordance with a previously established protocol [115] and expanded in complete medium, *i.e.* Alpha-minimal essential medium (αMEM) supplemented with 1 % antibiotics (100 U/ml penicillin and 0.1 mg/ml streptomycin, PS) and 10 % fetal bovine serum (FBS).

COL1 scaffolds were divided into four groups: scaffold only, scaffold functionalized with angiostatin, scaffold seeded with rBMSC and scaffolds functionalized with angiostatin and seeded with rBMSC. The groups with angiostatin were functionalized with 5 µg angiostatin diluted in 50 µl distilled water and pipetted onto the top of the scaffolds. Scaffolds with cells were seeded with 5×10^5 rBMSC.

4.3.2 Subcutanous implantation

The study was approved by the Norwegian Animal Research Authority. Scaffolds were implanted subcutaneously on the dorsum of 24 female Lewis rats (weight: 200 g, age: 12 weeks). Subcutaneous pockets were created by blunt dissection (Figure 3). One scaffold from each group was implanted and the wounds closed with resorbable sutures. After 2 and 8 weeks, the animals were euthanized by an overdose of CO_2. Samples were harvested and snap frozen in liquid nitrogen and stored at -80 °C until analysis.

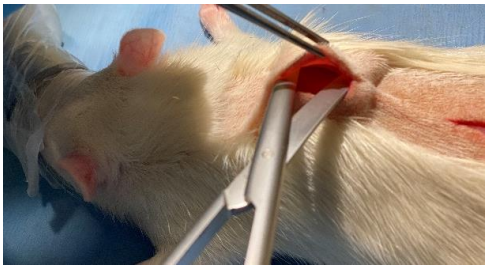

Figure 3. Image of stump dissection of subcutaneous pockets. Photo: Mohammed Ahmad Yassin.

4.3.3 Molecular & histological analysis

Samples harvested after 2 weeks were analysed with Real Time – Quantitative Polymerase Chain Reaction (RT-qPCR) and immunofluorescence staining for cluster of differentiation 31 (CD31) with quantification. Samples harvested after 2 and 8 weeks were analysed histologically.

4.4 Systematic review (Study II)

A review protocol was developed for a systematic review of the literature on scaffold-based regeneration of TMJ structures using preclinical animal models. The aim was to answer the specific PICO (population, intervention, comparison, outcome) question: in experimental animal models, does implantation of biomaterial scaffolds loaded with cells and/or GFs enhance regeneration of disc or osteochondral tissues, compared with scaffolds alone, without cells, and/or GFs?

Potentially relevant publications were identified by a specific search strategy of electronic databases (MEDLINE via PubMed, Web of Science, Google and Google Scholar). Published articles fulfilling the required criteria, up to and including November 2017, were included. Full texts were retrieved, and two authors screened the titles and abstracts.

The following information was retrieved: author(s), study design, animal species and number of animals used, observation time(s), cell source(s), -type(s) and -numbers,

scaffold biomaterial(s), GF(s), control group(s), outcome(s), main findings and conclusions.

The Animal Research: Reporting *In Vivo* Experiments (ARRIVE) guidelines were applied in a modified version to report quality assessment in a graded manner ('high', 'moderate' and 'low' [116]. The Systematic Review Center for Laboratory Animal Experimentation (SYRCLE) tool for animal studies was used to assess the risk of bias (RoB), graded as "high", "low" or "unclear" [117].

4.5 3D printing of gelatin scaffolds (Studies III & IV)

4.5.1 Preparation of gelatin hydrogel

A 10 % w/v hydrogel solution was prepared by mixing porcine gelatin type A (Sigma-Aldrich) with distilled water. The hydrogel was cooled in the refrigerator at 4 °C, reheated to 30 °C and printed in sixteen perpendicular layers, with a shift between every third and fourth layer to decrease the pore size (Figure 4). After printing, the hydrogel was frozen, freeze-dried, and crosslinked (Figure 5).

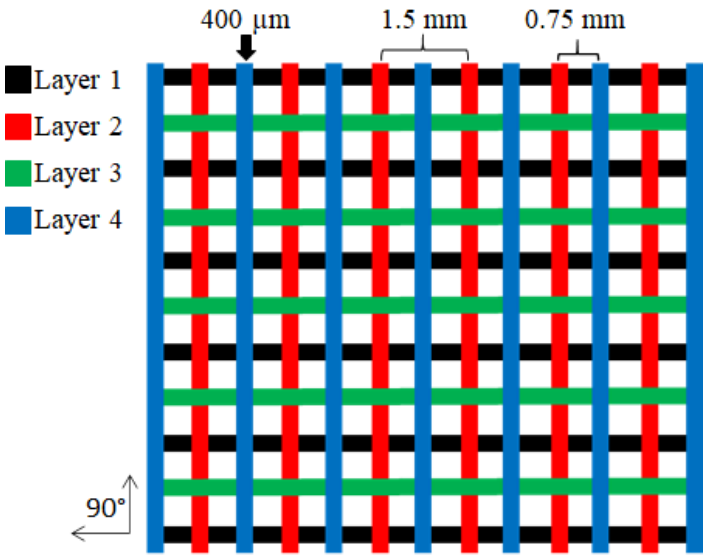

Figure 4. Schematic illustration of the printing design.

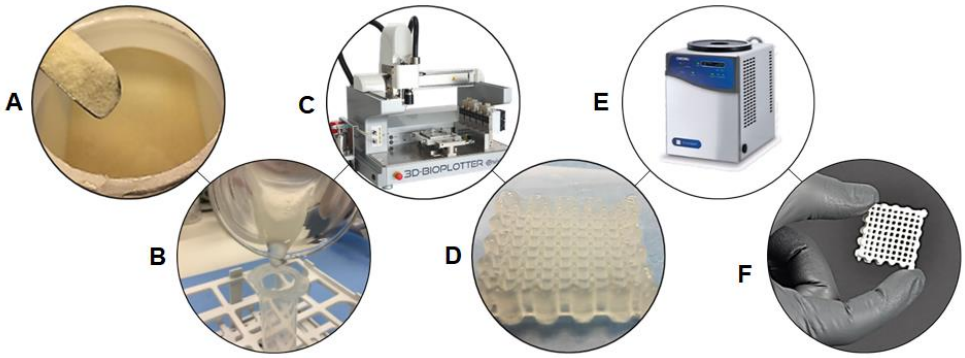

Figure 5. Steps in gelatin scaffold fabrication. Gelatin Type A powder (A), 10 % gelatin solution (B), 3D printing (C), 3D printed gelatin scaffold (D), freeze drying (E) and final scaffold (F).

Genipin (Study III)

Genipin (Wako) was dissolved in distilled water to a 1 % w/v solution under constant magnetic stirring in a 50 ml tube (40 ºC, 3 h). Scaffolds were crosslinked in 1 ml crosslinking solution for 48 h at room temperature. After crosslinking, the scaffolds were rinsed with PBS, frozen and freeze-dried (48 h, -52 °C, 0.014 mbar).

Dehydrothermal (Study IV)

In Study IV, freeze-dried scaffolds were shipped to collaborators at The Institute of Science and Technology for Ceramics (ISTEC, Milan, Italy). The scaffolds were subjected to heat treatment in an oven at 160 ºC under vacuum (48 h, 0.01 mbar).

Ribose (Study IV)

A 25 mM ribose solution was prepared by dissolving ribose in a solution of ethanol and phosphate buffered saline (PBS) at a ratio of 70/30 [118]. Freeze-dried samples were submerged in the solution in order to achieve a 1:1 ratio of gelatin and ribose, maintained at 37 °C for 5 days with gentle shaking. After ribose crosslinking, the scaffolds were freeze-dried with a cycle including two heating ramps, the first of 5 °C/h from -40 °C to -5 °C and the second of 3 °C/h to 20 °C for three days under vacuum conditions (0.086 mbar).

DHT + Ribose (Study IV)

Scaffolds were first crosslinked by DHT, and subsequently crosslinked by ribose as described above.

4.5.2 Degree of crosslinking (Study IV)

To determine the degree of crosslinking, the concentration of free primary amines (-NH_2) or carboxylic groups (-COOH) in non-crosslinked and crosslinked scaffolds was measured by a 2, 4, 6-Trinitrobenzenesulfonic acid (TNBS) assay, according to a previously reported protocol [119]. One ml of a 4 % (w/v) $NaHCO_3$ solution was added to each 5 mg of sample. Then, 1 ml of a freshly prepared solution of 0.5 % (w/v) TNBS was added after 30 min. The reaction mixture was heated at 40 °C for 2 h, before 3 ml of 6M HCl solution were added (60 °C, 90 min) to terminate the reaction. The reaction mixture was first diluted 1:1 with distilled water, before being cooled to room temperature. The absorbance at 415 nm was measured using a UV–visible spectrophotometer NanoDrop One C (Thermo Fisher Scientific). Blank control samples were prepared with the same procedure without scaffolds. The absorbance of the blank samples was then subtracted from each sample's absorbance. Measurements of all samples were run in triplicate.

The crosslinking percentage (CD) was evaluated using the following equation:

$$CD\ (\%) = (1 - \frac{Absorbance\ of\ crosslinked\ samples}{Absorbance\ of\ non-crosslinked\ controls}) \times 100$$

4.6 Structural characterization (Studies III & IV)

4.6.1 Micro computed tomography

Micro computed tomography (μCT, SkyScan) was used to evaluate the open porosity, surface area (mm^2) and surface volume (mm^3) of the scaffolds. For 3D reconstruction of the scaffolds, NRECON RECONSTRUCTIONVR CT software (SkyScan) was used.

4.6.2 Scanning electron microscopy

Crosslinked scaffolds were vacuum dried, sputter-coated with platinum and imaged (5 kV) using a scanning electron microscope (SEM, Jeol).

4.6.3 Swelling

Freeze-dried scaffolds were initially weighed in the dry state (W_0), before immersion in 10 ml of PBS at 37 ºC for 48 h (Study IV) and 72 h (Study III). At defined timepoints, swollen scaffolds were weighed (W_1). The liquid uptake was calculated according to the following formula:

$$Swelling\ (\%) = \frac{(W_1 - W_0)}{W_0} \times 100$$

4.6.4 Change in mass

For dynamic stability testing (Study III), freeze-dried scaffolds were weighed (W_0) before immersion in 10 ml of PBS at room temperature on a mechanical shaker. The PBS was changed after each timepoint (1, 3, 7, 14, 21 and 28 days). Samples were freeze-dried (48 h) and weighed (W_1, W_3...W_{28}), before re-immersion in PBS until the next timepoint. Mass loss was calculated using the following formula:

$$Change\ in\ mass\ (\%) = \frac{(W_0 - W_1)}{W_0} \times 100$$

For static stability testing (Studies III and IV), scaffolds were kept in 1 ml of complete medium, *i.e.* Alfa-minimal essential medium (αMEM) supplemented with 1 % antibiotics and 10 % FBS. The scaffolds were incubated (37 ºC in 5 % CO_2) for 7, 14, 21 (Study III) and 35 days (Study IV). The medium was changed twice a week. Three samples from each timepoint were imaged in a microscope (Leica M205 C) and freeze-dried for 48 h before weighing and imaging. The same formula as described above was used to calculate the percentage of mass loss.

For stability testing, scaffolds were weighed after freeze-drying (W_0) and immersed in 1 ml of complete medium in 24-well plates. The scaffolds were incubated (37 ºC

in 5 % CO_2) for 7, 14 and 21 days. The medium was changed twice a week. At the defined timepoints, samples were freeze-dried (48 h) and weighed (*e.g.* W_1). Loss of mass was calculated by the same formula.

4.6.5 Enzymatic degradation (Study IV)

The stability of crosslinked gelatin scaffolds was evaluated by an *in vitro* enzymatic degradation test, as reported previously [118]. Briefly, dry scaffolds were incubated in 1 ml 0.1M Tris-HCl (pH 7.4) containing 50 U/ml bacterial collagenase (Clostridium histolyticum, Type 1, Sigma-Aldrich), at 37 °C. The time required for complete digestion of non-crosslinked gelatin was 2 h. The scaffolds (n = 3 from each group) were freeze-dried, and their degradation was determined by UV-vis Spectrophotometer NanoDrop One C (Thermo Fisher Scientific) (see Eq.1). The percentage degradation of the samples was calculated with the non-crosslinked collagen considered to be 100 % degraded.

Eq.1 $$Degradation\ (\%) = \frac{A_f}{A_{ctr}} \times 100$$

A_f = absorbance after 2 h in collagenase solution of sample.

A_{ctr} = absorbance after 2 h in collagenase solution of non-crosslinked sample.

4.7 Mechanical testing (Studies III & IV)

Cylindrical scaffolds 10 mm in diameter of and 8 mm in height, with the same internal design, were printed and crosslinked, as previously described. Young's Modulus of the different crosslinked scaffolds was calculated from the linear part of the stress-strain curve. Creep tests (Study IV) were carried out at 0.03 MPa. After an isothermal period of 5 min at 37 °C, they were subjected to a defined stress for 15 min, before being left without any stress for 15 min.

4.8 Scaffold sterilization (Studies III & IV)

3D printed gelatin scaffolds fabricated for Study III were sterilized by 70 % ethanol for 30 min, followed by 2 h UV-light exposure and air-drying in a laminar flow hood. The scaffolds were washed with PBS to remove remnants of ethanol. For Study IV, scaffolds were sterilized by gamma irradiation and sterile packaged before use. All scaffolds were pre-wetted in complete medium and incubated for 24 h before seeding.

4.9 Cell culture

4.9.1 Cell isolation

Rat BMSC (Studies I & IV)

Ethical approval for obtaining rat cells was granted from the Norwegian Animal Research Authority. Cells were harvested and isolated in accordance with established protocols [115].

Human BMSC (Study III)

Ethical approval for obtaining human bone marrow was granted by the Regional Ethical Committees for Medical and Health Research Ethics. Parental informed consent was obtained according to ethical guidelines. The cells were isolated as previously described [54]. Aspirates were obtained from the iliac crest of two donors (7 and 12 years old) undergoing iliac crest surgery for cleft lip and palate reconstruction.

Cells for all experiments were cultured in complete medium (i.e. alpha minimum essential medium, containing 1 % antibiotics and 10 % fetal bovine serum); incubation was at 37 °C in 5 % CO_2, with changes of medium every third day.

4.9.2 *In vitro* tri-lineage differentiation and evaluation (Study III)

Multi-lineage differentiation was conducted according to previously described methods [54]. Chondrogenic and adipogenic differentiation were conducted in defined medium (Gibco) and osteogenic differentiation in complete medium supplemented

with 0.05 mM L-ascorbic acid 2-phosphate, 10 nM dexamethasone and 10 mM β glycerophosphate (Sigma-Aldrich). Briefly, adipogenic and osteogenic differentiation was investigated by culturing 7×10^3 and 3×10^3 hBMSC in 12-well plates for 14 and 21 days, respectively. The cells were washed with PBS and induced after 24 h by adding adipogenic and osteogenic medium. Chondrogenic differentiation was performed in 15 ml tubes with 1 ml of 5×10^5 cells in suspension, centrifuged and cultured as pellets for 28 days in chondrogenic medium. Complete medium served as the control for all cultures. Oil red O, Alizarin red and Alcian blue (Sigma-Aldrich) stainings were used to confirm lipid vesicles, calcium deposition and proteoglycan matrix for adipogenic, osteogenic and chondrogenic differentiation, respectively.

4.9.3 Indirect cytotoxicity (Study III)

The cytotoxicity of the crosslinker concentration was investigated by culturing hBMSC in genipin-extraction medium and comparing with control medium. The viability was evaluated using live/dead (Invitrogen) and alamarBlue (Invitrogen) assays after one and three days.

4.9.4 Formation of pellets and spheres (Study III)

Pellets were formed by suspending 3×10^5 hBMSC (passage 5) per ml of chondrogenic medium and distributed as 1 ml per 15 ml tube. Cell suspension was centrifuged (1200 rpm for 5 min) and incubated with the cap loosened to ensure gas exchange. After 24 h a spherical cell pellet was evident at the bottom of the tube.

Spheres were formed by using Aggrewell-400 microwell culture plates according to the manufacturer's instructions. Each well contained 1200 microwells, and 1.2×10^6 hBMSC per well were seeded, suspended in chondrogenic medium. The plate was centrifuged and 1200 spheres (1000 cells/sphere) were formed after 24 h of incubation (Figure 6). The spheres were cultured in the microwells for the entire culture period of 21 days.

Pellets served as a control for chondrogenic differentiation and spheres and scaffolds were compared to pellets with reference to gene expression, immunofluorescence and Alcian blue staining.

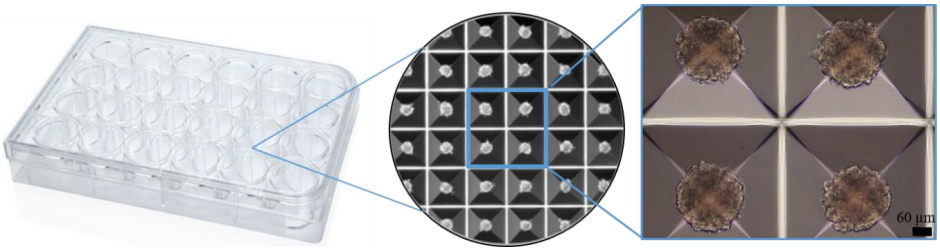

Figure 6. Illustration of microwell culture plates for spheres formation. Spheres imaged after 24 h (scale bar 60 µm).

4.9.5 Cell seeding of scaffolds (Studies I, III & IV)

Medium from the pre-wetting was discarded before cells were seeded using a 70 µl cell suspension. The cell suspension was distributed drop wise onto the top of the scaffolds. Cells were allowed to attach for 1 h before additional medium (430 µl) was added to the wells. The medium was changed every third day.

4.9.6 Cell attachment and seeding efficiency (Studies III & IV)

The morphology, density and attachment were assessed 4 h after seeding the scaffolds. Samples were fixed in 3 % GTA, vacuum dried, sputter-coated with platinum and imaged (5 kV) by SEM (Jeol). Seeding efficiency was calculated using a DNA-based cell proliferation assay (PicoGreen). The fluorescence units (FU) of the cells attached to the scaffolds and the cells remaining in the wells after seeding were compared to 2D controls seeded with the same cell number. Blank controls (empty wells) and scaffolds without cells were subtracted from the FU before the calculations. Cell seeding efficiency, based either on the cells on the scaffold (sc) (Study III) or cells remaining in the wells (w) (Study IV), was calculated according to the following formula:

$$Cell\ seeding\ efficiency_{sc}\ (\%) = \frac{(\mathrm{FU_{sc}} - \mathrm{FU_{blank}})}{\mathrm{FU_{2D}}} \times 100$$

$$Cell\ seeding\ efficiency_w\ (\%) = 100\% - [\frac{(\mathrm{FU_{sc}} - \mathrm{FU_{blank}})}{\mathrm{FU_{2D}}} \times 100]$$

4.9.7 Cell distribution (Study III)

To investigate the distribution of cells on the scaffolds, they were cultured for 1 and 4 days in basal medium, fixed in 10 % formalin for 15 min, washed with PBS and permeabilized with 0.1 % Triton-X (in PBS) for 10 min, then incubated with Alexa Fluor 488 Phalloidin (Thermo Fischer Scientific) diluted in PBS (1:50, 40 min in the dark). Cell nuclei were stained with 4′,6-Diamidino-2-phenylindole dihydrochloride (DAPI) in PBS, 1:3000, for 10 min in the dark. After washing with PBS, the scaffolds were imaged using a 3D confocal microscope (Dragonfly 505).

4.9.8 Cell viability (Studies III &IV)

The cell viability on the seeded scaffolds was evaluated after 1 and 4 days using live/dead staining (Invitrogen) according to the manufacturer's protocol. Briefly, 1.5 µl green staining was mixed with 5 ml PBS, before adding 1.5 µl red staining. Medium was discarded from the wells and the scaffolds were washed with PBS. After 45 min incubation in the dark, the scaffolds were examined in a fluorescence microscope (Nikon Eclipse 80i).-

4.9.9 Cell proliferation (Studies III & IV)

Proliferation of BMSC on scaffolds was investigated by DNA quantification (PicoGreen) after culture in basal medium (2×10^5 cells) and in differentiation medium (1.2×10^6 cells) for seven days. FLUOstar OPTIMA (BMG Labtech) was used for plate reading of the fluorescence units (FU).

4.9.10 RT-qPCR (Studies I, III & IV)

RNA was extracted following the protocol from Maxwell (Promega) and measured using NanoDrop 1000 Spectrophotometer (Thermo Fischer Scientific). A standardized

amount (ng) of RNA was used for cDNA synthesis using High-Capacity cDNA Reverse Transcription Kit (Applied Biosystems) and SimpliAmp Thermal Cycler (Applied Biosystems). For PCR, TaqMan Fast Universal PCR Master Mix (Applied Biosystems) and StepOne RT-PCR System (Applied Biosystems) were used for gene expression detection. Glutaraldehyde 3-phosphate dehydrogenase (GADPH) was used as an endogenous control. Table 2 presents the genes and their roles.

Table 2. Gene primers used in the thesis

Gene (Study)	**Name**	**Role**
IL1A (I)	Interleukin 1 alpha	Active in cartilage degeneration [120].
IL1B (I)	Interleukin 1 beta	Activates and recruits macrophages. Active in cartilage degeneration [120].
SOX9 (I, III, IV)	SRY-box 9	Main chondrogenic transcription factor [62]
ACAN (I, III, IV)	Aggrecan	Cartilage-specific core protein. Major structural component of cartilage. Regulated by SOX9 [64].
COL1 (I, III, IV)	Collagen type 1	Main collagen component of fibrocartilage [7].
COL2 (I, III, IV)	Collagen type 2	Main collagen component of hyaline cartilage. Trace amounts in fibrocartilage [7].

COL3 (I)	Collagen type 3	Fibrocartilage marker controlling fibril diameter of COL1 [121]
COL10 (III, IV)	Collagen type 10	Hypertrophy marker expressed by terminal phenotype of CC undergoing endochondral ossification [67].
VEGF (I)	Vascular endothelial growth factor	Stimulates angiogenesis and endothelial cell migration and proliferation [122].
PECAM1 (I)	Platelet endothelial cell adhesion molecule	A major constituent of blood vessel forming cells, endothelial cells [43].

4.9.11 Histology (Studies I, III & IV)

For histological analysis in Study I, the harvested tissue was embedded in Optimal Cutting Temperature compound (Tissue-Tek). Cryosections of 5 μm thickness were made and mounted on glass slides. Samples were stained for hematoxylin and eosin (H&E) and Masson's Trichrome (MTC) and blindly described by a pathologist.

4.9.12 Immunofluorescence staining (Studies I & III)

In Study I, samples, after 2 weeks implantation were stained with immunofluorescence for CD31 and quantified. Cryosections were fixed using ice cold acetone for 10 min, before blocking for 1 h in 10 % normal goat serum (NGS in PBS). Primary antibody, mouse anti-rat (BD Bioscience), was incubated (1:50 in 10 % blocking buffer) overnight at 4 °C. Secondary antibody (Santa Cruz, sc-2092) was incubated (1:200 in 10 % blocking buffer) for 2 h at room temperature, in the dark. Sections were quantified for CD31+ region of interest (ROI) divided by total ROI, using a TIRF

microscope (Nikon Eclipse 80i) and digital software (NIS-Elements Advanced Research Software).

In Study III, scaffolds, spheres and pellets were fixed in 10 % formalin for 15 min and washed with PBS. Sections were mounted on polysine-treated glass slides to ensure adequate adhesion. Spheres and pellets were treated with 0.1 % Triton-X for 30 min and blocked in 10 % NGS for 1 h, both at room temperature in 1.5 ml tubes. Primary antibody for SOX9 (Abcam 185966, rabbit monoclonal antibody, 1:200 diluted in 10 % NGS) and COL1 (Abcam 34710, rabbit polyclonal antibody 1:500 in 10 % NGS) were incubated overnight at 4 °C. After washing with PBS, SOX9 and COL1 were conjugated with secondary antibody Alexa Fluor 488 (goat anti-rabbit, ThermoFischer Scientific) and incubated (1:200, SOX9 and 1:800, COL1) for 2 h at room temperature.

All the immunofluorescence stainings were combined with DAPI (1:3000, 10 min in the dark) to stain the nuclei. Spheres and pellets were imaged using a 3D confocal microscope (Dragonfly 505). Sections of scaffolds were imaged using a TIRF-microscope (Nikon Eclipse 80i).

4.9.13 Glycosaminoglycan assay (Study IV)

Sulphated glycosaminoglycan (sGAG) assay (Blyscan) was conducted according to the manufacturer's protocol. Briefly, samples were snap frozen after 21 days of culture and stored at -80 °C. Samples were thawed and transferred to 1.5 ml tubes with 1 ml Papain Extraction Reagent and placed in a shaking water bath (65 °C, 60 rpm) for 3 h of digestion. Samples were centrifuged and supernatant collected. Of the supernatants, 100 µl were pipetted into new 1.5 ml tubes, before 1 ml Dye reagent was added and incubated in room temperature for 30 min on a mechanical shaker (60 rpm). This resulted in the formation of a sGAG-dye complex. The tubes were then centrifuged. The sGAG-dye complex formed a pellet, and the supernatant was removed carefully to avoid disturbing the complex. To dissolve the complex, 500 µl Dissociation Reagent was added and vortexed for 10 min. For measurements, 200 µl of each sample were pipetted into individual wells of a 96-well plate. Plate readings were performed using Varioskan (Thermo Fischer) measuring the absorbance with a wavelength of 656 nm.

4.10 Statistical analysis (Studies I, III & IV)

In Study I, a Shapiro-Wilk test on the residual from the univariate one-way analysis of variance (ANOVA) was used to test the normality. For the non-normally distributed data (COL1), a non-parametric test (Mann-Whitney *U* test) was applied. To determine intergroup statistical significances, a Tukey's post-hoc comparison of the mean using SPSS Statistic 25 (IBM, Armonk. NY, USA) was performed. In Studies III and IV, ΔCt-values were used in a mixed-effects model with regression to calculate the difference between the timepoint within the groups. One-way ANOVA was used to detect intergroup statistical differences at the same timepoints, using STATA (version 16, StataCorp, College Station, TX, USA). The results were presented as box plots with median and 95 % confidence interval. Inter- and intragroup statistical significance was set to p-values ≤ 0.05. All quantitative data are presented as mean ± standard deviation (SD), unless stated otherwise. Graphs and plots were made using GraphPad Prism (version 7.04).

5. Summary of main results and general discussion

Strategies for regeneration of lost or damaged TMJ cartilage can be classified as scaffold-free and scaffold-based [30]. Scaffold-free approaches involve *in vitro* self-assembly and self-organization processes, which are intended to simulate *in vivo* development of cartilage by the cells and to replicate the native morphology [123]. These approaches rely on a high density and proximity of the cells to facilitate cell-to-cell communications and stimulation of ECM-secretion [123]. Potentially, this produces biochemically mature and mechanically robust structures pre-implantation, which integrate more readily [83]. In orthopaedics, harvesting CC before *in vitro* self-assembling and re-implantation in articular cartilage defects (*i.e.* ACI) is an established method [124]. There are however, few such methods for TMJ regeneration. A successful scaffold-free approach by injection of nasal CC for regeneration of TMJ condyle resorption has been reported [40]. As this is a minimally invasive method, both injection and ACI risk uneven distribution and leakage of cells. The method is therefore limited to minor defects [125]. Another example of a scaffold-free approach is the use of aggregated cell cultures, *e.g.* pellets, regarded as the standard method for chondrogenic differentiation of MSC *in vitro* [67]. However, massive cell numbers are required and output is low, because only one pellet is cultured per tube. More recently, smaller-sized aggregates, *i.e.* spheres, have been reported to enhance the stemness, survival and differentiation potential of MSC [73]. This method allows for high-throughput manufacturing of uniform size-controlled spheres facilitated by microwell platforms [77].

While scaffold-free approaches are promising, especially for regenerating minor defects [42], for larger defects scaffold-based strategies provide greater structural support. Depending on the source material(s), scaffolds can be tailored to accommodate regional differences in porosity and stiffness and can be functionalized with cells and/or biomolecules [30]. Scaffolds serve as carriers for cell-transplantation and offer a temporary 3D framework on which cells can form a new matrix, and also provide a template for endogenous cell recruitment [123].

Ideally, the rate of scaffold degradation should match the rate of neotissue formation, without provoking uncontrolled inflammatory reactions. The mechanical properties of the scaffold should be equal to the native structures it is intended to replace [30]. These stringent requirements underline the importance of appropriate biomaterial(s) selection. Polymers, both natural and synthetic, are frequently used for CTE [86]. While natural polymers, e.g. collagen and gelatin are generally biocompatible and biodegradable and simulate native ECM more closely than synthetics, they often lack the durability of the native tissues. Alternatively, synthetic polymers can be more readily tailored with respect to degradation rates and mechanical properties, which are important properties in case of reconstruction of complex structures with regional variations [87]. However, they tend to be hydrophobic and their acidic degradation products can provoke uncontrolled inflammatory responses [86].

COL1 is the main component of fibrocartilage [7]. It exhibits excellent biocompatibility, biodegradability, hydrophilicity and cell attachment properties and is widely used as a scaffold biomaterial for CTE [91]. Gelatin also exhibits the above properties, but with less antigenicity and at a lower cost [97]. Moreover, gelatin is thermo-reversible, with superior hydrogel-forming properties to collagen. Gelatin can therefore be used for 3D printing. However, without proper crosslinking, the natural polymers exhibit poor stability and mechanical properties.

The main focus of this thesis was to explore scaffold-based approaches to regeneration of the cartilaginous structures of the TMJ, using natural polymers and BMSC. In Study III, pellets and spheres were included for comparison of scaffold-free alternatives for TMJ regeneration.

5.1. The *in vivo* effect of angiostatin functionalized collagen (Study I)

There are few studies of the role of vascular inhibition in regeneration of naturally avascular structures [81]. An untoward consequence of vascularization of cartilaginous structures could be mineralization, such as endochondral ossification, which might

endanger the stability of the implants [43]. Study I was therefore undertaken in order to investigate the vascular inhibiting effects of angiostatin and its potential for chondrogenic differentiation of MSC cultured on collagen scaffolds, in an ectopic rat model.

At the gene level, the expression of VEGF (Figure 8A) and PECAM1 (Figure 8B) was downregulated in the angiostatin groups 2 weeks after implantation. This was confirmed by immunofluorescence staining and quantification of CD31 positive areas (Figure 7). VEGF is associated with CC hypertrophy during endochondral ossification [126]. Moreover, VEGF-inhibition has been proposed as a promising target molecule for treatment of chronic closed lock [127]. The results of Study I are in accordance with those of Centola et al., reporting similar lower CD31+ cell infiltration using fibrin-hyaluronan scaffolds, functionalized with bevacizumab, a VEGF-inhibitor, seeded with nasal chondrocytes [43].

Vascular levels are closely associated with inflammation [128]. After two weeks *in vivo*, angiostatin downregulated the gene expression of the inflammatory markers IL1A (Figure 8C) and IL1B. Elevated levels of these markers have been reported in patients with degenerative TMJ diseases [129]. Therefore, functionalization of implanted scaffolds with factors which could decrease the levels of inflammatory cytokines may be promising means of re-establishing homeostasis of the TMJ and initiating a regenerative process.

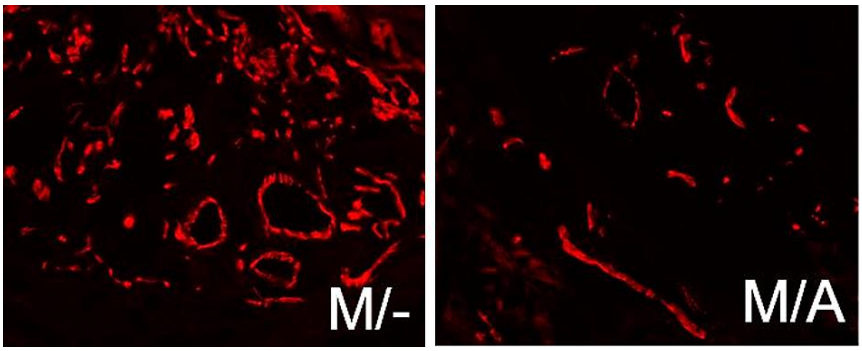

Figure 7. Immunofluorescence staining for CD31 (red signal) after 2 weeks' implantation. M/-, scaffolds loaded with MSC; M/A, scaffolds functionalized with angiostatin and loaded with MSC.

The potential of Angiostatin to promote chondrogenic differentiation of MSC-seeded collagen scaffolds *in vivo*

SOX9 is an essential transcription factor for chondrogenesis [130]. The fact that heterozygous mutations in SOX9 can lead to severe chondrodysplasias [131], highlights its importance. It regulates the expression of both ACAN [64] and COL2 [65], both important components of cartilage. ACAN is a core protein vital for GAG formation, which contributes to the mechanical toughness of cartilage [66]. Although angiostatin-functionalized scaffolds supported expression of cartilage-specific genes, the levels were downregulated (non-significantly). The decreased levels of ACAN (Figure 8E) and COL2 can be linked to the downregulation of SOX9 (Figure 8D), but the fibrocartilage-related gene COL1 was also influenced (Figure 8F). IL-1 is reported to decrease the levels of SOX9 in CC [132], which was the same effect observed for angiostatin on MSC.

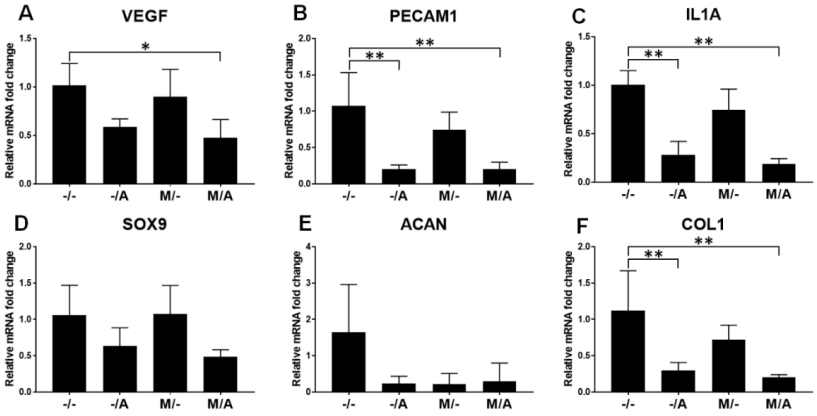

Figure 8. A selection of gene markers for vascularization (A-B), inflammation (C) and fibrocartilage specific genes (D-F) for Study I. -/-, scaffold only; -/A, scaffolds functionalized with angiostatin; M/-, scaffolds loaded with MSC; M/A, scaffolds functionalized with angiostatin and loaded with MSC; *, $p < 0.05$; **, $p < 0.01$.

Histologic examination revealed that implants from all groups were surrounded by a thin fibrous capsule, supporting biocompatibility of the scaffold material (Figure 9). Multinucleated giant cells (MNGC) are commonly observed with engulfed degradation products [133] and this was apparent in all groups. The blinded, descriptive histological evaluation by a pathologist, revealed a higher presence in the angiostatin groups. The differences had decreased after 8 weeks, indicating complete degradation or release of angiostatin. The increase of MNGC in the angiostatin-groups may be related to the use of a human recombinant type and is not in agreement with the findings of Centola *et al.* of an inhibitory effect of the monoclonal VEGF-antibody, bevacizumab, on macrophage migration [43].

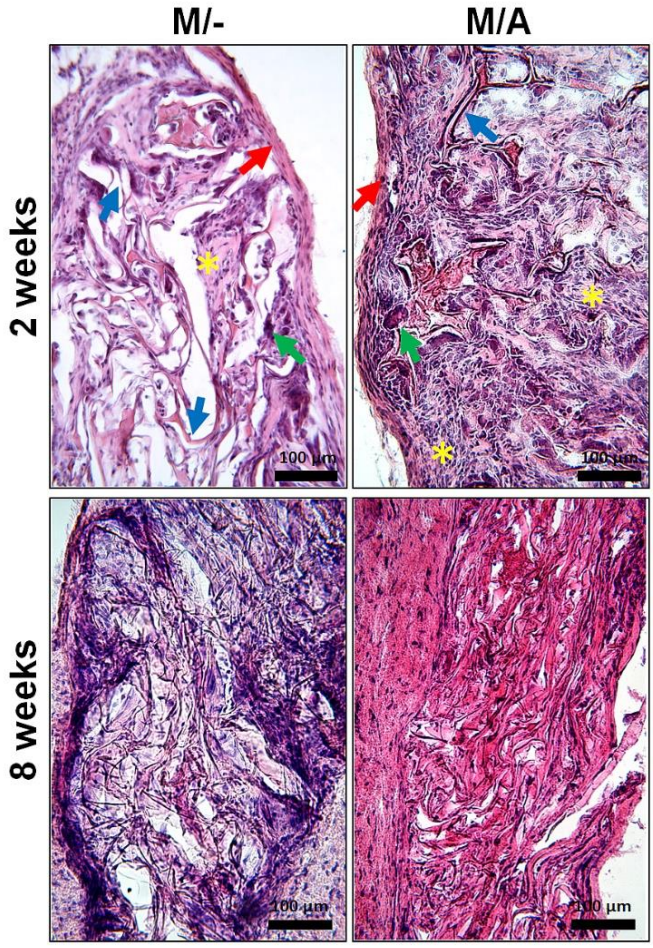

Figure 9. A selection of histological images (Haematoxylin and eosin staining) after 2- and 8-weeks implantation. Fibrous capsule (red arrows), scaffold pores (blue arrows), multinucleated giant cells (green arrows), mononuclear inflammatory cells (yellow asterix). M/-, scaffolds loaded with MSC; M/A, scaffolds functionalized with angiostatin and loaded with MSC.

While all groups demonstrated new collagen matrix formation (Figure 9), the group with scaffolds functionalized with angiostatin and seeded with MSC ('M/A') revealed the greatest, after 8 weeks. The contribution of the implanted MSC to matrix formation was expected. However, the histology does not correspond with the gene levels after 2 weeks, as the control group with scaffold only ('-/-'), had the highest expression of COL1, COL2 and COL3. This illustrates the difficulty of selecting timepoints and the

importance of histological evaluation of the newly formed tissues. Despite matrix formation in all groups, there was no evidence of cartilage. This can be explained by the use of undifferentiated MSC in an ectopic site, in the absence of endogenous signals or mechanical stimulation [134]. Others have successfully engineered ectopic cartilaginous structures, using CC and preconditioning scaffolds *in vitro* with anti-angiogenic factors [43]. By seeding the scaffolds with mature cells like CC, with the capacity to secrete cartilaginous matrix, ectopic cartilage formation using angiostatin might be possible. As functionalization of scaffolds with angiostatin to supress vascularization was not sufficient, incorporation of inductive GFs in the scaffold [87], could be a strategy to induce MSC *in vivo*.

Similar strategies, with different factors have been reported for articular CTE. Sun *et al.* [80] used non-viral transfection of MSC with endostatin seeded on collagen scaffolds. MSC were successfully transfected and produced potentially therapeutic levels of endostatin *in vitro*. Jeng *et al.* [81] used endostatin-plasmid-supplemented collagen scaffolds seeded with MSC and CC for cartilage repair. In contrast to angiostatin's effect on MSC *in vivo*, endostatin-supplemented collagen scaffolds did not prevent chondrogenesis of co-cultured cells *in vitro*. The impact of combining CC with BMSC has been demonstrated clinically in a phase-I trial using allogenic BMSC and autologous CC (with pericellular matrix) in a 90:10 or 80:20 ratio, respectively. The ratio ws dependent on the amount of available CC for harvest at the site of injury and the mix was combined with fibrin-glue to adhere to focal articular cartilage defects in 10 patients [58]. After 12 months there were no signs of allogenic cells in the defect and the authors suggested that the paracrine effect of MSC stimulated the structural and functional restoration of the cartilage.

In Study I, the dose and release of angiostatin were not optimized, and this must be considered a limitation that may have influenced the fate of the implanted MSC. Moreover, the cell seeding density was in the lower range considered optimal for *in vitro* CTE and fibrochondrogenesis [135]. Failure to achieve mature cartilage formation in this study and the observed lack of established methods for TMJ cartilage regeneration reinforced the need for a thorough literature review of established

knowledge within the field of *in vivo* TMJ TE. A systematic review was therefore undertaken to assess the limitations and potential of scaffold-based cartilage regeneration, with special reference to the scaffold material, shape, cell types and animal models.

5.2. **Systematic review (Study II)**

Systematic reviews and meta-analysis can be helpful in providing an overview of a specific topic or field, and for planning future studies. Animal experiments need to be well designed, conducted and analyzed in order to provide reliable results [136]. Systematic reviews can improve methodology and provide valuable information about previous work and experience. In contrast to narrative reviews, which include studies based on expert opinions, a systematic review is intended to answer a focused research question by including studies which meet pre-defined criteria [136]. Thus, systematic reviews are more objective and comprehensive with respect to the use of sources and databases for inclusion of studies. The impact of summarizing research findings with a high level of evidence and well-designed interventional studies is high, and systematic reviews and meta-analysis are therefore generally considered to be the highest level of scientific evidence.

In conclusion, the results of the systematic review showed that strategies including implantation of biomaterials with cells and/or GFs, were superior to biomaterials alone. Implantation of a scaffold only was superior to an empty defect or no implant. Further, differentiated MSC were superior to undifferentiated cells. However, the included studies lacked consistency: more standardized methods and quantitative reporting of data would facilitate comparison and meta-analysis of the results.

5.2.1 Systematic review of animal models

The systematic review included 30 studies of both small (n = 25) and large (n = 5) animal models. The included studies, published in the period 1994-2017, comprised both ectopic (*i.e.* subcutaneous) and orthotopic models in five different species (Table

). The sample sizes varied from 2-60, and the observation times from two weeks to 12 months.

Table 3. Number of studies of the different models and species

		Mice	Rabbits	Dogs	Goats	Sheep	Total
Ectopic	*SM*	1					**12**
	Disc	3					
	Condyle	8					
Orthotopic	*Disc*		6	2			**18**
	Condyle		7		2	1	

SM, synovial membrane.

Small animals, like mice, that often constitute a starting point for proof of principle studies [112], have advantages such as lower costs and easier housing and handling [113]. The potential to control the genetic background results in less variation and reduces the number of animals needed to obtain statistically valid data [137]. All ectopic models included subcutaneous implantation in mice, in experiments into regeneration of TMJ disc, condyle or synovial membrane. Cell-seeded scaffolds (most commonly BMSC) demonstrated regeneration outcomes superior to cell-free scaffolds, and differentiated cells were better than undifferentiated cells. The latter conclusion is transferable to Study I, in which undifferentiated BMSC did not form ectopic cartilage matrix. However, the heterogeneity of the studies made comparison of the results difficult. Rodent size limits feasibility for orthotopic models, because of the physical difficulty of the surgical approach [138, 139]. It is of interest to note however, that investigators at Massachusetts General Hospital (MGH) recently published a thorough guide to mouse TMJ anatomy and surgical approach for orthotopic TMJ regeneration [140]. Despite the disadvantage of size, this well-described protocol is a valuable guide to the planning and conduct of future orthotopic *in vivo* studies in rodents.

Rabbit was the most frequently reported species for orthotopic models. Rabbits have many of the advantages of rodents, but their size allows for easier surgical access. Two included studies reported disc defect models, where surgical perforations were created, and scaffolds implanted. This model is analogous to the critical-sized defect models

often used in BTE. It is easier to secure the implant in site, compared to a total disc replacement model, which is more susceptible to displacement [88].

It should be noted that spontaneous healing of defects in orthopedic rabbit models has been reported [141] and evidence of regeneration should therefore be interpreted with caution. However, the regeneration could be controlled for by including group(s) with an empty defect/no implant for base-line comparison. Other disadvantages of rabbits are related to the anatomy, movement and loading, which differ considerably from the human TMJ [141], which makes it less than ideal for translational purposes.

Although no animal model can fully replicate the clinical setting, the results from large animal models are considered to be more readily translational with respect to therapeutic efficacy [137]. Dogs, sheep, and goats were all included in the review. However, they all have advantages and disadvantages. Dogs are carnivores, with higher loading on the TMJ than sheep and goats (herbivores) and pigs (omnivores) [114]. With respect to jaw movements, the TMJ in dogs mainly rotates, while sheep and goats have primarily translational jaw movements [114]. Pigs have both rotational and translational jaw movements, and are reported to be the species with TMJ function, anatomy and morphology most closely resembling that of humans [142]. However, in addition to the general drawbacks of large animal models, such as costs and handling difficulty, farm pigs exhibit inferior growth of the zygomatic arch, which obstructs lateral preauricular access to the TMJ [142]. Combined with the further disadvantage of continuous growth until 18 months [114], this might explain the absence of pig models from the review.

A recent publication used a self-assembly scaffold-free strategy using allogenic CC for regeneration of a TMJ disc defect in a minipig model [42]. Although minipigs have a slower growth rate than farm pigs, they pose the same challenge of inferior growth of the zygomatic arch, hindering preauricular surgical access [142]. Therefore, a posterolateral approach was used to create a defect resembling the clinical condition of early-stage disc-thinning. In a preliminary study of a disc defect model, implant fixation had failed, highlighting the difficulty of adequate anchorage of an implant

which is subject to rotational and translational movements. Despite the need for a further surgical intervention to harvest CC and the associated risk of donor-site morbidity, the authors recommended the costal ribs as a clinically attractive source of CC, based on their abundant availability and their potential to produce a robust ECM with high mechanical integrity [143].

5.2.2 Cells and biomaterials in the systematic review

Several different cell types were reported. Adult MSC were reported in 12 studies, with BMSC most frequent (n = 12). CC were reported in six studies, either alone or in combination with BMSC, fibroblasts or osteoblasts for ectopic condyle regeneration. Adult MSC from other sources such as adipose tissue, synovial tissue and condylar fibrocartilage, were also described. Whole bone marrow and fibroblast-like synoviocytes were less frequently reported. The ideal cell source for TMJ TE remains unclear. However, BMSC are attractive candidates. They are: more readily available than CC, exhibit minimal donor-site morbidity, are well-characterized and are reported to have greater chondrogenic differentiation potential than ASC [54].

Of the various scaffold biomaterials reported (Table 4), natural polymers (n = 17) were the most frequent, followed by synthetic biomaterials (n = 10). The remaining studies used a combination of natural and synthetic biomaterials (n = 3). Most of the scaffolds were either commercially available products or fabricated by traditional methods, *e.g.* freeze-drying, moulding or salt-leaching. Only a minority were fabricated by 3D printing technology. The first reported study was from 2005, by Schek *et al.* [144] using indirect solid free-form fabrication to create a cylindrical mould for a condyle scaffold. The bone-phase scaffold was created by casting hydroxyapatite (HA) followed by sintering, and the polymeric scaffold (PLA) was created by salt-leaching in the same mould. The bi-phasic scaffold was bonded by solubilized PLA. The ceramic scaffold was seeded with bone morphogenetic protein 7 (BMP-7) gene transfected fibroblasts and the polymeric scaffold with CC. Ectopic implantation successfully resulted in bone and cartilage formation in the bi-phasic scaffold with a mineralized interface. This is another example of the importance of using differentiated

cells in an ectopic site. Such a result is difficult to achieve with a scaffold-free approach.

Table 4. Overview of scaffold biomaterial(s) and application according to year of publication of the included studies.

Year	Application	Material(s); GFs	Reference
1994	Disc	PLA+PGA	[145]
1996	Condyle defect	Gelatin + (Fib/Throm 1:1)	[146]
2000	Condyle defect	Collagen	[147]
2001	Condyle	PLA+PGA+Pluronic+$CaSO_4$	[148]
2002	Condyle defect	Collagen; rhBMP-2	[149]
2002	Condyle	Coral, natural	[150]
2003	Condylectomy	PLA+PGA+Gelatin; rhBMP-2	[151]
2003	Condyle	PEDGA	[152]
2004	Disc defect	Collagen	[153]
2005	Disc defect	Collagen/ subdermal grafts	[154]
2005	Condyle	PEDGA	[155]
2005	Condyle	PLA+HA	[144]
2007	Condyle defect	Collagen; FGF-2	[156]
2010	Condylectomy	UB-ECM+Collagen	[157]
2011	OC defect	Pluronic F-127	[158]
2011	OC defect	PLGA	[159]
2011	Condyle defect	PLGA; TGF-B1 +BMP-2	[160]
2011	Condyle	Coral	[161]
2011	Disc	UB-ECM	[162]
2012	Condyle	Coral	[163]
2012	Disc	UB-ECM	[164]
2013	Disc	PLA	[88]
2013	Condylectomy	HA+Collagen+PRP	[165]
2014	Synovial membrane	Collagen	[166]
2014	Disc defect	Fibrin+Chitosan	[167]
2015	Disc defect	Collagen	[168]
2016	Disc defect	PCL+PLGA	[87]
2016	Disc	Collagen/Gelatin/Matrigel	[45]
2017	Condyle	CCS, PCL/HA, PGA+PLA	[169]
2017	Disc defect	Collagen	[170]

CAD/CAM, computer aided design/computer aided manufacturing; CCS; cartilage cell sheet; FGF, fibroblast growth factor; Fib, fibrinogen; GFs, growth factors; HA, hydroxyapatite; OC, osteochondral; PCL, polycaprolactone; PLA; poly lactide acid; PGA, poly glycolic acid; PLGA, poly lactic-co-glycolic acid; PRP, platelet-rich

plasma; rhBMP-2, recombinant bone morphogenetic protein-2; TGF-b, transforming growth factor beta; Throm, Thrombin; UB-ECM, urinary bladder extracellular matrix.

The next publication using 3D printing for TMJ TE in an animal model was not reported until 2016. Tarafder *et al.* [87] printed polycaprolactone (PCL) + poly lactic-co-glycolic acid (PLGA) scaffolds with incorporated microspheres of growth factors (GFs) for TMJ disc defects in rabbits. By incorporating a combination of transforming growth factor β3 (TGF-β3) and connective tissue growth factor (CTGF) in the scaffolds, successful regeneration of disc perforations was observed after 4 weeks without implanted cells – compared to GF-free scaffolds. This illustrates the endogenous regenerative cell potential in an orthotopic site and the power of advances in fabrication methods for tailoring the scaffold properties, with temporal release of GFs. The strategy of GF-functionalized scaffolds could hold promise for ectopic differentiation of MSC in Study I.

Based on the review findings, it was decided to continue using a natural polymer scaffold to ensure biocompatibility and biodegradability, in combination with BMSC. Furthermore, 3D printed scaffold fabrication was selected on the basis of the promising results from one of the most recent publications [87]. This would allow the scaffold geometry to be customized and the porosity to be controlled. Moreover, the cell density used in Study I would need to be increased and *in vitro* chondrogenic differentiation of BMSC would be required.

5.3. **3D printing of gelatin (Studies III & IV)**

Natural polymer hydrogels are able to simulate native ECM. Considering the abundance of COL1 in fibrocartilage, it would have been logical to continue using the biomaterial from Study I. However, collagen is expensive, with slow gelation, making it less than ideal for 3D printing, which involves considerable 'trial and error' [97]. Gelatin has the same advantages of biocompatibility and cell-adhesion properties [97, 171], but hydrolysis of COL1 combined with well-controlled manufacturing processes makes it less antigenic [97]. Moreover, gelatin is far less expensive, exhibits high

gelation for hydrogel formation and is reported to show promise for CTE [94, 172]. It is thus an attractive candidate for 3D printed scaffold fabrication for TMJ TE. Gelatin has been used in three of the studies included in the systematic review, but in all cases combined with other polymers – and none for 3D printing. Gelatin has been used in scaffold biomaterials for a variety of applications [94], from regeneration of adipose tissue [172], liver tissues [173], nerve tissue and cardiac tissue constructs to bone, among others [94]. For CTE, gelatin has been used as a constituent in composite scaffolds, freeze-dried porous scaffolds [108] and hydrogels [174]. Nevertheless, there are few studies reporting the application of gelatin hydrogel for TMJ TE.

When 3D porous scaffolds of gelatin are made by electrospinning and freeze-drying, there is only limited capacity to control the macroscopic pores. A major advantage of 3D printing is the ability to control macroporosity [175]. Layer-by-layer hydrogel 3D printing is a rapidly advancing method [176]. It provides high accuracy, controlled macroporosity and the potential to customize scaffolds to fit the defect [176]. Freeze-drying of the 3D printed hydrogel scaffold results in dual porosity, as the printed pores are accompanied by the microscopic pores of the strands.

3D printing of gelatin requires a high material concentration with consequently high viscosity and decreased printability [177]. For this reason, gelatin has been blended with different biopolymers to enhance the viscosity [177, 178]. Gelatin can form gels at temperatures below 30 ºC, facilitated by the transformation of the random coiling of the molecules to triple helical formations [97]. This thermo-reversible property demonstrates a memory of viscosity [179], and cooling the hydrogel to jelly in the refrigerator before heating it to printable temperatures increases the printability, compared to cooling down a heated gel. In the current project, large structures with 16 well-defined layers of 10 % gelatin were successfully printed without co-deposition of other materials. The printed project was designed by software (Bioplotter RP) and the object was sliced horizontally at a thickness of 80 % of the nozzle size, as recommended by the manufacturer. This was done to allow for the decrease in vertical dimension due to the overlap of the soft polymer strands (Figure 10). The application of a 400 µm nozzle resulted in layers of 320 µm thickness.

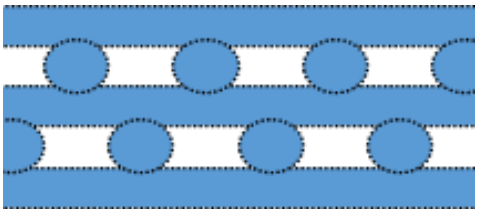

Figure 10. Schematic illustration of the overlap of the printed strands in the vertical dimension.

The ratio between the inner nozzle diameter and the printed strands revealed an increased spreading ratio of the strands from layer two to layer 8 and layer 16 (Figure 11). The overall spreading ratio was 1.3, compared to the theoretical strand width of 400 µm. The increased strand width can be linked to the heightened distance between the nozzle and the cooled platform (4 °C) leading to less thermal stabilization of the strands. Furthermore, any discrepancy between the strand thickness and the sliced digital object will accumulate throughout the process. For optimal printing accuracy, the ratio should be 'one'. This is very challenging when printing hydrogels – and despite the comprehensive optimization of the printing parameters, there is potential for improvement.

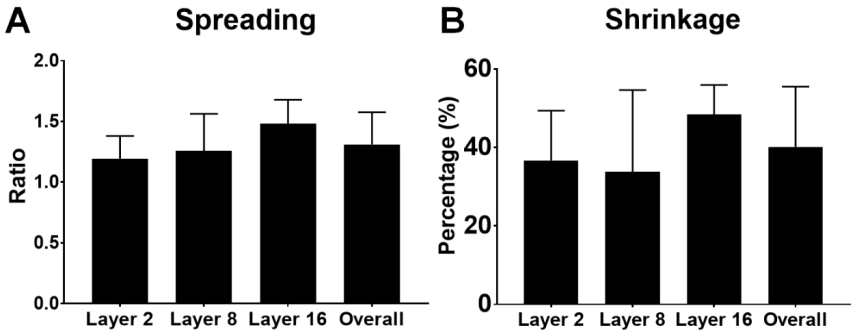

Figure 11. Spreading ratio (A) during printing and shrinkage (B) after freeze-drying of layer 2, 8, 16 and overall.

5.4. **Crosslinking of printed gelatin scaffolds (Studies III & IV)**

Because of its thermo-reversibility, gelatin depends on proper crosslinking to avoid dissolving in a physiological environment and to improve the mechanical properties [180]. Traditional crosslinkers such as GTA have disadvantages, for example cytotoxicity of the agents and their degradation products, due to the aldehyde groups [181, 182]. Therefore, optional natural crosslinkers were explored. As a result of the crosslinking reactions, the white freeze-dried scaffolds changed color (Figure 12). Genipin resulted in a dark blue color, due to the pigment formation from the covalent bond formation with the primary amines [103, 171]. DHT resulted in a light-yellow color from the physical crosslinking, ribose in a dense yellow color from the chemical reaction, while the dual crosslinking resulted in something in-between closer to ribose.

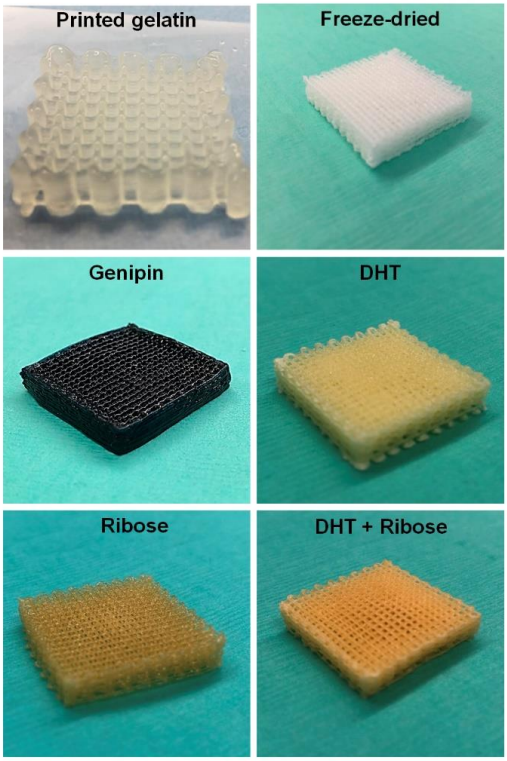

Figure 12. Gross images of printed hydrogel, freeze-dried scaffolds, and crosslinking by genipin, DHT, ribose and dual crosslinking with DHT + ribose.

5.5. **Degree of crosslinking, swelling & degradation**

Genipin is reported to be an efficient crosslinker of different natural polymers. The reaction can be controlled by the concentration and duration of incubation [183]. Solorio *et al.* [183] prepared 6 % (w/v) gelatin (Type A and B) microspheres for GFs encapsulation using 1 % (w/v) genipin and measured the degree of crosslinking. Gelatin type A reached a plateau of 90 % after 24 h, higher than Type B (50 %). De Clercq *et al.* [184] reported approximately 75 % crosslinking of Type B gelatin microspheres crosslinked by 1 % genipin. The effectiveness of genipin has been explained by the 'range' of the crosslinker. In short-range crosslinks, genipin can chemically react with amino groups within a gelatin molecule and between two adjacent gelatin molecules. Genipin can also establish long-range intermolecular crosslinks and consume two free amino groups [185].

In Study IV, the degree of crosslinking was measured as a percentage of crosslinked primary amines. DHT had the lowest degree of crosslinking at 14.5 ± 1.9 %, compared with 31.8 ± 5.6 % for ribose. Highest were the dual-crosslinked samples at 44.4 ± 8.5 %. This is close to the sum of the two single crosslinkers and demonstrates the differences in crosslinking mechanisms. In DHT treatment, the high temperature, combined with pressure, removes bound water and results in intermolecular crosslinks as a result of amide formation or esterification [108]. Ribose chemically induces intermolecular bridges between the lysine residues of one gelatin molecule and the arginine residues of other gelatin molecules [118]. By combining the two methods, the number of crosslinked amines increased. The effect of ribose crosslinking can be adjusted by the concentration, reaction time and temperature [186]. At 32 %, the degree of crosslinking was higher than reported in the literature for 1 % collagen (26 %), crosslinked by the same protocol but with a higher ribose concentration [118]. The values are comparable, but the difference could be due to structural differences between collagen and gelatin. A study comparing DHT and genipin (1.5 %) crosslinking of 5 % (w/v) type A gelatin using the same protocol, revealed a marginally higher degree of crosslinking from genipin (31 %) than DHT (30 %) [108]. However, the variations in the published data on the degree of crosslinking of gelatin-genipin structures can be

attributed to variations in the type of gelatin, the concentrations of gelatin or genipin, the shape and size of the structures as well as the time and temperature of the crosslinking.

After printing, the hydrogel was frozen, leading to ice crystal formation of the water molecules. Freeze-drying evaporated the crystalized water and resulted in micropores in the strands. This led to shrinkage of the initial printed strand dimensions as measured in Study IV. DHT treatment resulted in the highest shrinkage. This could be attributed to the physical treatment of heat under vacuum, which removes additional bound water from the samples. Ribose treatment includes freeze-drying before and after crosslinking. This resulted in less shrinkage than DHT. It is noteworthy that the least shrinkage was observed in dual-crosslinked samples exposed first to DHT treatment, followed by ribose and freeze-drying. However, the variations in shrinkage did not significantly affect differences in object volume, surface area or open porosity measured by μCT. The porous strands from the freeze-drying process were evident in all groups and confirmed by SEM. However, SEM also disclosed differences in the micro-porosity. Crosslinking by genipin (Figure 13A) in Study III resulted in smooth-surfaced porous strands. In Study IV (Figure 13B), DHT treatment resulted in lamellar pores, while ribose resulted in more spherical pores. Dual crosslinking resulted in the smallest and most homogeneous porosity.

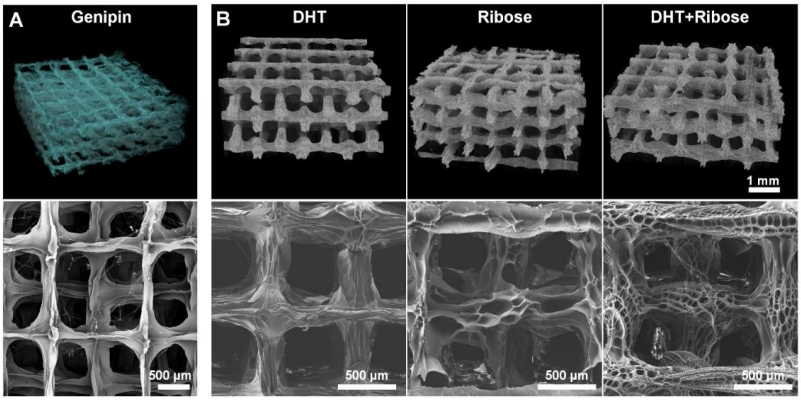

Figure 13. Micro CT 3D-reconstruction of the scaffolds and SEM images from genipin-crosslinked scaffolds in Study III (A) and DHT, ribose and dual-crosslinked scaffolds in Study IV (B).

Gelatin is degraded by hydrolysis and enzymatic actions [97]. Enzymatic resistance is important in a physiological environment, to avoid excessively rapid degradation. In Study IV (Figure 14), the dual crosslinking method with the highest degree of crosslinking resulted in the least enzymatic degradation (13.5 %). It was of interest to note that DHT, with the lowest degree of crosslinking (61.6 %) was more resistant to collagenase than ribose (79.4 %), indicating that physical crosslinked gelatin is less susceptible to collagenase. Crosslinking with ribose can be performed before (pre) or after (post) freeze-drying. Comparisons of the methods with collagen have shown post freeze-drying, as conducted in Study IV, to be superior [118]. Enzymatic degradation was not measured for the gelatin scaffolds in Study III. However, comparison of different crosslinkers on gelatin sponges (4 % v/w) revealed enzymatic resistance of genipin to collagenase type I to be comparable to the GTA, but with markedly higher cell viability and proliferation [180].

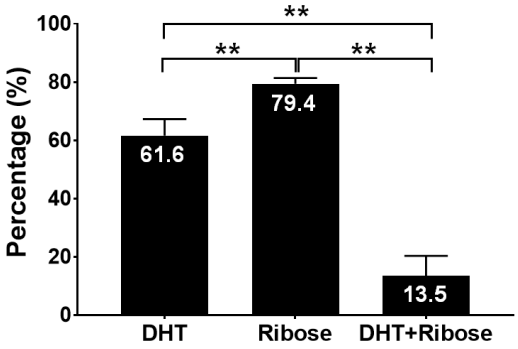

Figure 14. Enzymatic degradation of crosslinked scaffolds by DHT, ribose and DHT+ribose. **, $p < 0.01$.

The capacity to swell is one of the advantages of using hydrophilic porous scaffolds, as they can absorb surrounding fluids, *e.g.* cell culture medium *in vitro* and synovial fluid *in vivo*, nourishing the cells and simulating the native ECM. The porous strands of all the crosslinked scaffolds had high swelling capacity (Figure 15A). This was measured as mass gain over time. Of all the crosslinked scaffolds, genipin (Study III) had the lowest values after 48 h (364 %). In Study IV, ribose had the highest water

uptake, with a swelling of 1343. 3 ± 200.8 % weight gain after 48 h, while swelling of 848.3 ± 57.4 % and 828.8 ± 69.2 % was recorded for DHT and dual-crosslinked scaffolds, respectively. The superior swelling capacity of ribose can be attributed by the hydroxyl groups introduced by the sugar, and their ability to form hydrogen bonds to water molecules [187]. Dual crosslinking with DHT seemed to diminish this effect. The swelling properties can also be related to the degree of crosslinking, as it affects the free amine groups available for binding water [187], and it may indicate that genipin has a higher degree of crosslinking than DHT.

The stability of the scaffolds was tested in basal medium (Figure 15B). After 14 days, genipin-crosslinked scaffolds (Study III) were outperformed by the dual-crosslinked scaffolds (Study IV), which were the most stable after 21 days of culture. The genipin and the ribose-crosslinked scaffolds had the same percentage of mass loss, while the DHT scaffolds were the least stable at all timepoints. The inferior stability of DHT treated samples in complete medium, compared to ribose, correlates with the degree of crosslinking, but not with the enzymatic resistance, as ribose treated samples were more susceptible to collagenase. These results are not in concordance with Shankar *et al.* [108], reporting that under physiological conditions, DHT crosslinked gelatin was more stable than genipin – despite the comparable extent of crosslinking. However, in the referred study, genipin had superior swelling properties to DHT, which may explain the increased hydrolysis. Furthermore, the superior stability of genipin crosslinked scaffolds compared to the DHT could be related to differences in degree of crosslinking, which would correlate with the inferior swelling capacity [108].

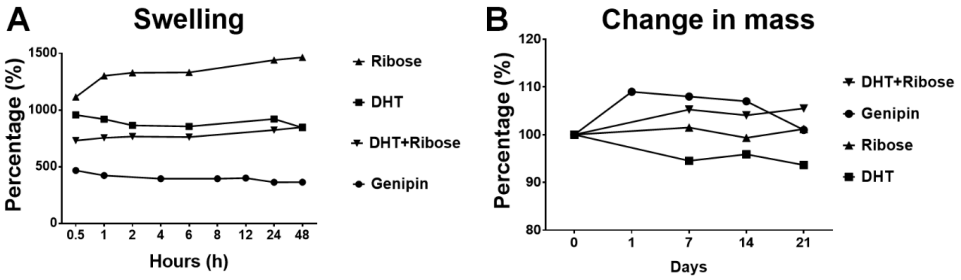

Figure 15. Swelling properties (A) and stability in complete medium of the differently crosslinked scaffolds for 21 days. Note: Genipin was conducted in a separate experiment (Study III) and the experimental conditions may not have been exactly the same as the others.

5.6. **Crosslinking affects the mechanical properties of 3D printed gelatin scaffolds (Studies III & IV)**

During normal function, the fibrocartilaginous structures of the TMJ are subjected to dynamic forces. Scaffolds for such applications should be characterized in terms of mechanical properties [7]. In Study III, the compressive modulus in a dry state was higher for non-crosslinked scaffolds (9.49 ± 3.93 MPa) than for those crosslinked with genipin (4.52 ± 1.51 MPa). In wet conditions, the non-crosslinked samples collapsed and were not measurable, and the genipin crosslinked samples dropped to 191 ± 0.01 kPa (Figure 16). After maximum compression of the dry samples and 2 min rehydration in PBS, the genipin crosslinked samples fully recovered their initial dimensions, while there was minimal recovery of the non-crosslinked samples (3.75 %). In Study IV, the DHT crosslinked samples had the highest Young's Modulus (37.6 ± 13.3 kPa) in wet conditions and ribose had the lowest values (2.0 ± 0.5 kPa), significantly lower than DHT and dual-crosslinked samples (30.9 ± 10.9 kPa) (Figure 16).

For load-absorbing structures, elastic properties and the ability to revert to the original dimensions after deformation are important. It can also be beneficial for surgical implantation in sites with limited access, as they can be compressed into place. To test the stress-relaxation properties, a creep test was undertaken in Study IV. After

continuous loading for 15 min the ability of the samples to revert to their original dimensions was investigated. The strain values of DHT were 53 % immediately after release of the load and decreased to 7 % after 15 min recovery. The strain values for ribose and dual-crosslinked samples were 19 % and 14 % after loading, and 16 % and 12 % after recovery, respectively. The dual-crosslinked samples, with the greatest degree of crosslinking, exhibited the highest modulus of elasticity. Based on the mechanical characterization, this can be attributed to the DHT treatment, rather than ribose.

These findings are not in accordance with reports in the literature, whereby genipin (16.2 ± 0.3 kPa) is reported to be inferior to DHT (54.4 ± 3.8 kPa) crosslinked scaffolds [108]. However, the results were achieved under different experimental conditions. Although, both tests were conducted in a wet state, the scaffolds in Study IV were soaked for 24 h at 37 °C pre-testing, as in the reported protocol [108]. This makes the comparison of Studies III and IV less valid, and favors an overestimation of mechanical properties of the genipin crosslinked samples. Nevertheless, the values are far from those of the native TMJ disc and condylar cartilage, which limits potential applications to defects rather than to load bearing structures [6, 188].

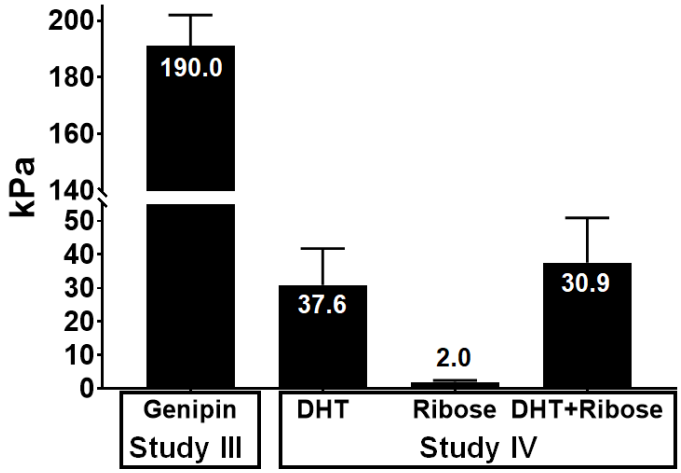

Figure 16. Young's Modulus of the different crosslinked gelatin scaffolds.

5.7. **BMSC characterization and cell aggregate formation (Study III)**

When cells are isolated from new donors, it is important that donor variation is taken into account, by characterizing differentiation capacity *in vitro* [54]. In Studies I and IV rBMSC were sourced from the biobank at the Department of Clinical Dentistry, UiB. The uniform genetic background and controlled housing conditions of rats, circumvents the issue of donor variability associated with human donors [189].

In Study III, hBMSC from two donors were used. The adipogenic and osteogenic differentiation potential of hBMSC was confirmed via Oil red O staining (Figure 17A) of intracellular lipid vesicles (14 days) and Alizarin red staining (Figure 17B) of calcium deposits (21 days), respectively; no staining was observed in non-induced control cells.

While adipogenic and osteogenic differentiation were investigated in monolayers, chondrogenic differentiation was tested in 3D pellet cultures. Aggregation of MSC is considered essential for chondrogenesis, simulating the developmental stages of embryogenesis [190]. This facilitates cell-to-cell contact through adhesion proteins (*e.g.* N-cadherin), which activates intra- and extracellular signaling pathways essential for MSC chondrogenesis [191]. Paraffin sections of chondrogenically induced hBMSC stained positively for Alcian blue (Figure 17C) after 28 days, demonstrating synthesis of cartilaginous proteoglycan matrix [54], while the pellets cultured in control medium had a more irregular shape and pale staining.

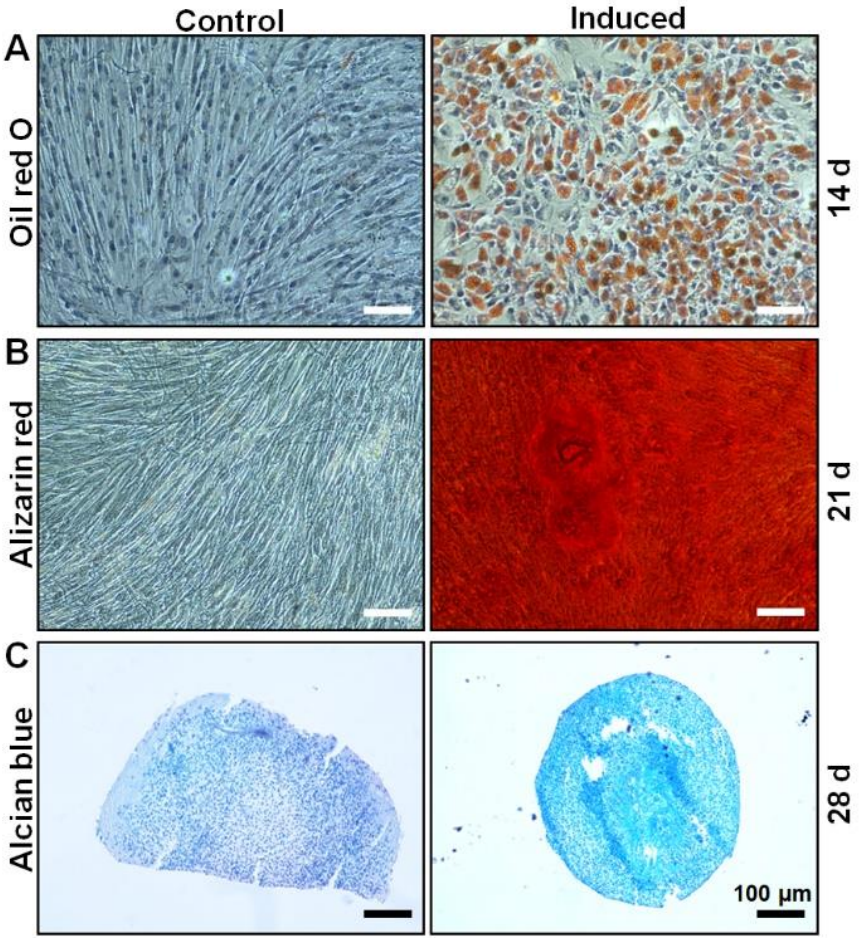

Figure 17. Staining of hBMSC cultured in control and (A) adipogenic, (B) osteogenic and (C) chondrogenic defined medium.

The cell pellets and spheres formed during the first 24 h after centrifugation in tubes and microwell plates, respectively (Figure 18). The pellets were visible at the bottom of the tubes as white, rounded aggregates of approximately 1 mm diameter. The spheres were localized at the bottom of the microwells, uniform in size and shape, with a diameter of approximately 250 µm. Live/dead assay after 1 and 4 days revealed viable cells in both aggregated cultures, but with an increasing number of dead cells after 4 days.

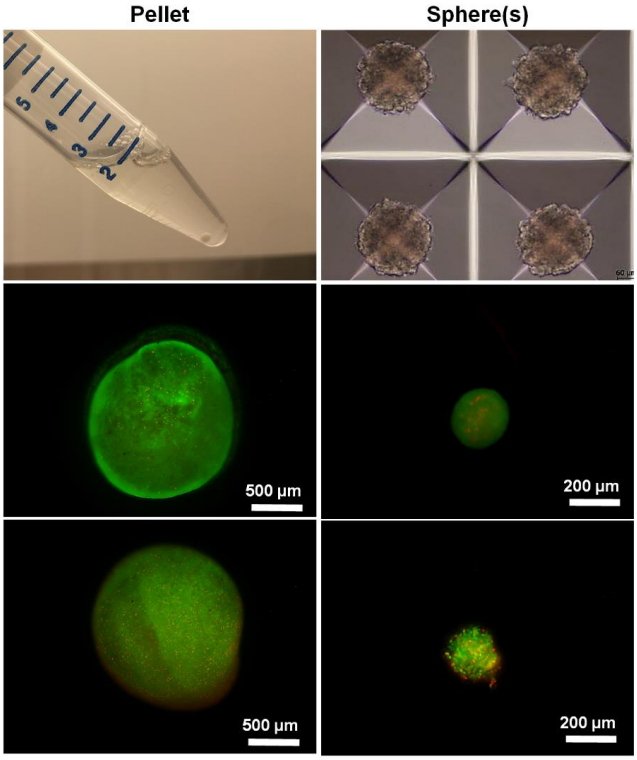

Figure 18. Images of pellet and sphere(s) after 24 h (top), live/dead assay after 1 day (middle) and 4 days (bottom). Red signal (dead cells), green signal (living cells).

5.8. **Indirect cytotoxicity testing of genipin (Study III)**

Because of the cytotoxicity of traditional crosslinkers, *e.g.* GTA, genipin has been used as an alternative for crosslinking of several biomaterials [181, 192]. Genipin is a natural compound, derived from hydrolysis of the *Gardenia* fruit and is reported to be 10 000 times less toxic than GTA [181]. The cytotoxicity of genipin is however, reported to be dose-dependent [193]: hence in Study III, the cytotoxicity of 1 % genipin (v/w) to hBMSC was investigated.

Cell cultures of hBMSC monolayer in genipin-extraction medium and control medium demonstrated similar trends with respect to proliferation and viability. As measured with alamarBlue, both groups proliferated significantly from day 1 to day 3. The cell-

morphology was similar (Figure 19A), and the viability of the hBMSC, equal (Figure 19B). It was concluded that at the applied concentration of 1 %, genipin was non-cytotoxic for hBMSC.

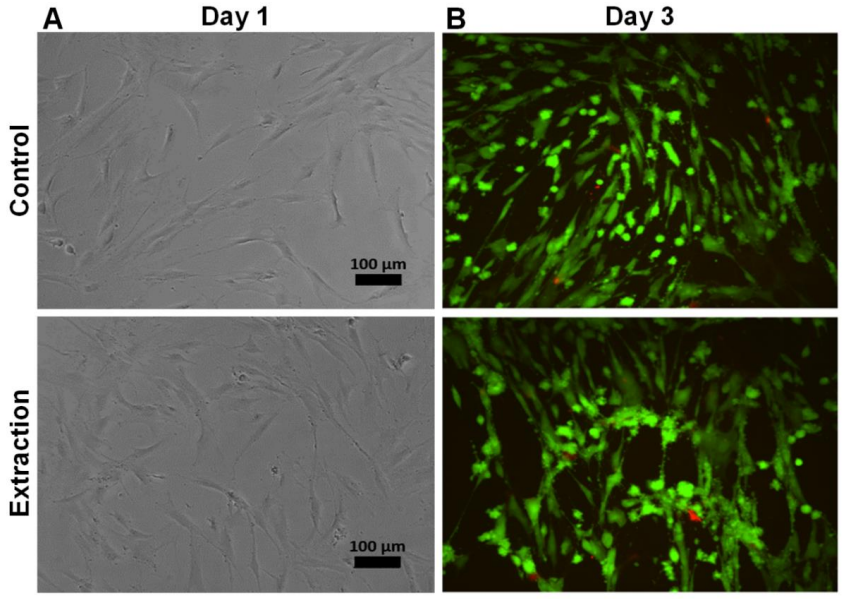

Figure 19. Morphology (A) and live/dead staining (B) of hBMSC cultured in control medium and genipin extraction medium. Red signal (dead cells), green signal (living cells).

5.9. **Cell-scaffold interactions (Studies III & IV)**

Cell seeding is a crucial step for *in vitro* cell cultures on 3D scaffolds [194]. To facilitate growth and differentiation, the seeded cells should be widely distributed and attached throughout the pores of the scaffold. The optimal cell seeding density of BMSC differs, depending on the targeted tissue and lineage of differentiation. Generally, chondrogenic differentiation requires a higher cell density than osteogenic differentiation, given that the cells require proximity for cell communication and differentiation. Bornes *et al.* [135] investigated the optimal seeding density of BMSC for *in vitro* chondrogenic differentiation. Monolayer expanded BMSC were seeded

onto collagen scaffolds in the range of 0.5-50 × 10^6 cells/cm^3. Based on gene expression, histological staining and GAG quantification, the authors concluded that the optimal range for hyaline CTE was from 5-10 × 10^6 cells/cm^3, while the lower range of 1-5 × 10^6 cells/cm^3 was optimal for fibrocartilage-related COL1 expression. The selected seeding number of 1.2 × 10^6 cells per scaffold (4.8 × 10^6 cells/cm^3) is at the upper range of the recommended seeding density for fibrocartilage.

In porous scaffolds, seeding efficiency is rarely 100 %, as some cells fail to attach and are lost from the structure. The printed design of the scaffold, with open macroporosity, led to lower cell seeding efficiency than for moulded and freeze-dried scaffolds with smaller, closed pores which can entrap more cells. Regardless of fabrication method, cell seeding efficiency is important in order to estimate the actual cell numbers attached to the scaffolds. In Study III, 57.3 % of the seeded hBMSC attached to the scaffold. This was higher than observed for the rBMSC in Study IV on DHT crosslinked scaffolds (51.6 %). Ribose- and dual-crosslinked scaffolds were significantly lower, at 34 % and 38 %, respectively.

The shift for every third and fourth layer of the scaffolds created physical barriers which facilitated cell attachment sites. This strategy has been reported to be a simple means of increasing the cell seeding efficiency of 3D printed scaffolds [195]. However, the reported cell seeding efficiency of less than 60 % can be linked to the porosity. Ribose had the largest pores and lowest cell seeding efficiency. Using the same strategy with PCL scaffolds, Declercq *et al.* [195] increased the cell seeding efficiency from 52 % to 66 %. However, these scaffolds had a porosity of 66-70 %, compared to 87-93 % for the different gelatin scaffolds. By decreasing the strand distance, the seeding efficiency could be improved. However, this led to decreased printability and reproducibility of the structures, as the strands tended to adhere to each other when the nozzle changed direction in the x-y plane.

The morphology of the attached cells was documented by SEM (Figure 20). Images after 24 h attachment revealed intergroup differences. Cells attached to ribose appeared more rounded and clumped whereas the others exhibited more spreading, spindle-

shaped morphology. This could be related to the stiffness of the material, attributable to the different crosslinkers, as ribose was the mechanically weakest material in wet conditions.

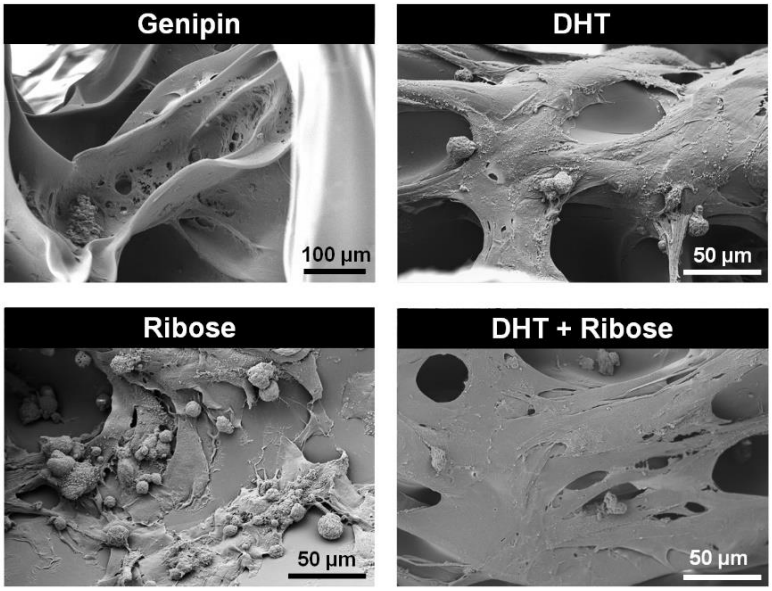

Figure 20. SEM images of cells attached to the different crosslinked gelatin scaffolds.

To evaluate the distribution on the scaffolds (Study III) fluorescent staining (phalloidin and DAPI, Figure 21) were used. Cells were observed both on the surface and in the depths of the porous scaffold.

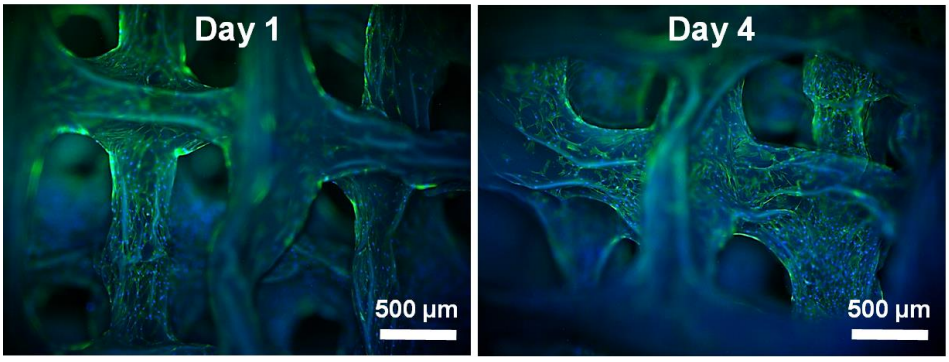

Figure 21. Cell distribution on genipin crosslinked scaffolds after 1 and 4 days. Green signal (phalloidin/actin), blue signal (DAPI, nuclei).

Viability of hBMSC (Study III) and rBMSC (Study IV) on the scaffolds was evaluated by live/dead assay (Figure 22). Qualitatively, all scaffolds supported cell viability and distribution after 1 and 4 days. Cross-sections and bottom view disclosed cell distribution through all layers. In Study IV, cells observed on the ribose crosslinked scaffolds were less viable than those on the DHT and dual-crosslinked scaffolds. This may be related to the differences in cell seeding efficiency, as no differences in dead cells were observed. Based on these findings, it was concluded all the crosslinker agents used for the 3D printed gelatin scaffolds were non-cytotoxic.

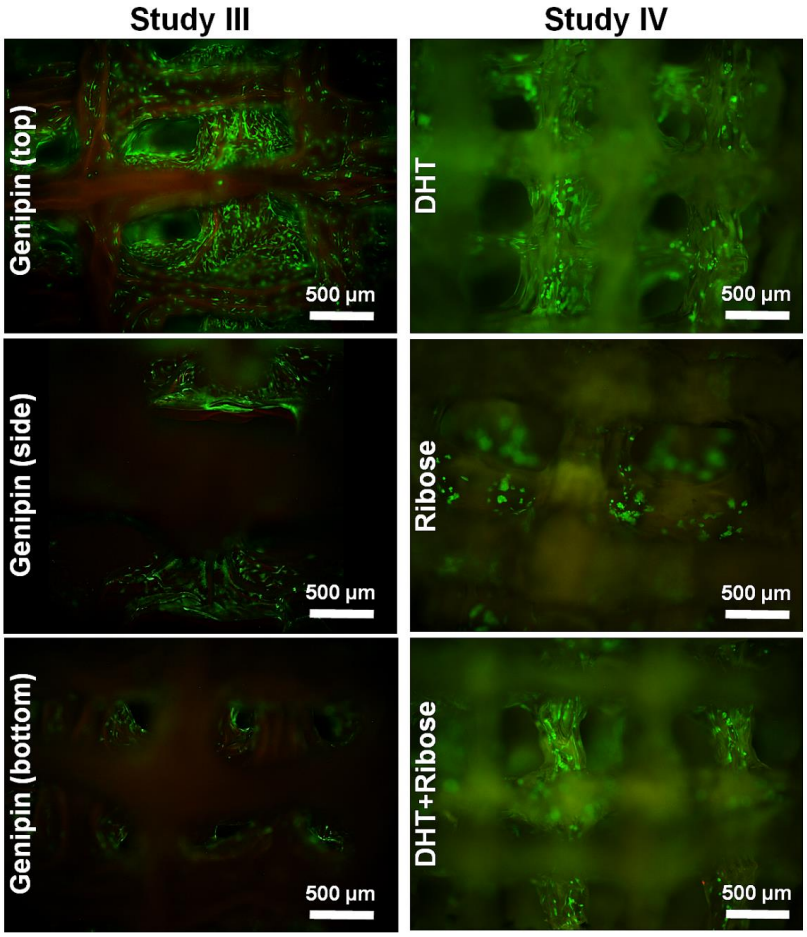

Figure 22. Cell viability after 1 day for Studies III and IV. Red signal (dead cells), green signal (living cells).

Cell-seeded scaffolds from all groups (Studies III and IV) supported cell proliferation from day 4 until day 7 in basal medium. Chen *et al.* [196] reported that the stiffness of the gelatin scaffolds affected CC proliferation. This may explain the poorer proliferation of rBMSC on ribose crosslinked scaffolds, compared to the significantly higher proliferation on the dual-crosslinked scaffolds. Another explanation is the scaffolds' ability to resist cellular contraction and retain their porosity, which stimulates cell proliferation [196].

5.10. Chondrogenic differentiation of BMSC (Studies III & IV)

All groups in Study IV supported gene markers for chondrogenesis and hypertrophy after 7 and 21 days (Figure 23). The main chondrogenic transcription factor, SOX9, was stable in all groups, with the highest, though non-significant level in the DHT group. Expressions of ACAN, the cartilage-specific proteoglycan core protein, were equal at day 7 and decreased significantly in all groups after 21 days. This explains the minimal GAG-formation after 21 days in all groups. Despite the significantly higher ACAN expression in dual-crosslinked scaffolds after 21 days, differences in GAG-formation were non-significant. This could indicate inadequate differentiation of rBMSC to the chondrogenic phenotype, as others have reported 3-fold higher GAG formation after 14 days of culture of CC seeded DHT crosslinked gelatin scaffolds [108]. The smaller scaffold porosity (390 ± 14 μm) may also have influenced the outcome. At 21 days, DHT had significantly higher COL1 expression than ribose, with intermediate levels of expression by the dual-crosslinked scaffolds. The ratio of COL1 to COL2 is one of the main differences between hyaline and fibrocartilage [7]. While fibrocartilage contains mainly COL1, hyaline cartilage is dominated by COL2. In the current study, COL2 expression was upregulated, while COL1 was stable or decreased (ribose) – indicating differentiation towards hyaline cartilage rather than fibrocartilage. The hypertrophy marker, COL10, was stable and close to equal in all three groups.

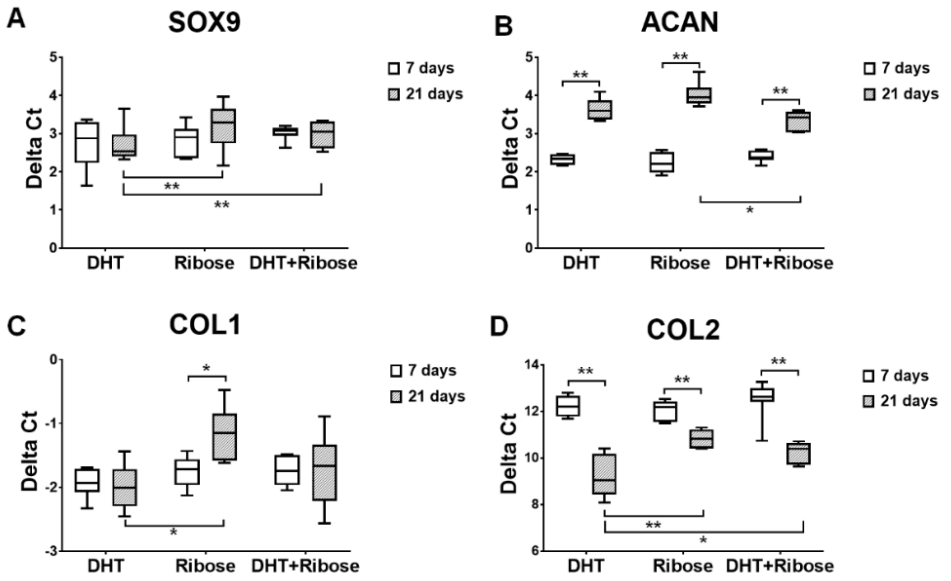

Figure 23. Gene expression of a selection of gene-markers in Study IV. *, $p < 0.05$; **, $p < 0.01$.

In Study III, hBMSC pellets served as a reference group. Compared to both the pellet and the sphere group, gene expression for all markers was lower in the scaffold group, at all timepoints. These findings were most pronounced for the chondrogenic markers SOX9 and ACAN. This can be related to the differences in the 3D microenvironments and is in accordance with reports in the literature, that spheres have superior differentiation potential [197]. Although in a 3D environment, cells cultured on scaffolds are further apart and dispersed than in the aggregated cultures. The morphology of the cells in the pellets and spheres was more condensed and spherical – while cells cultured on the scaffold appeared spread and spindle-shaped, more closely resembling a monolayer manner. Furthermore, the aggregated cultures induce mild hypoxia, activating hypoxia-related cascades, such as upregulation of cell-adhesion molecules (*e.g.* HIF-1α) involved in mesenchymal chondrogenesis [198].

Despite the lower expression of chondrogenic genes in the scaffold-group, upregulation followed the same trends and chondrogenic differentiation was confirmed by

immunofluorescence (SOX9 and COL1, Figure 24). After 21 days, the hypertrophy-related marker, COL10, was highly upregulated, particularly in the spheres (80-fold), but also in the pellets (20-fold). It was of interest to note that COL10 was expressed marginally in the scaffold-group (2-fold). Upregulation of COL10 is one of the challenges for chondrogenic differentiation of MSC, as it is reported to serve as a framework for subsequent calcification of articular cartilage [199]. This argument has been used to justify the use of mature CC, despite donor-site morbidity and the need for further surgical intervention [38]. Therefore, the ability of genipin crosslinked scaffolds to limit hypertrophy of differentiated hBMSC may be important for future experiments and may achieve successful cartilage maturation without calcification of the engineered constructs.

Alcian blue staining was positive for all groups. Qualitatively, the staining intensity was highest for spheres, followed by pellets and scaffolds. Sarem *et al.* found a direct correlation between the initial aggregate cell number and acceleration of chondrogenic differentiation, independent of extrinsic inductive factors [190]. They gradually reduced the cell numbers from 5×10^5 to 70×10^4 per pellet, demonstrating that the smallest aggregates stained positive for GAG formation using Alcian blue, even after 7 days in the absence of TGF-β1. In Study III, non-induced spheres were not cultured, but this study provides evidence of GF-independent activation of the chondrogenic program in MSC, by limiting the size of the aggregates. This intrinsic activation can therefore explain the superior GAG formation of the spheres and the lower chondrogenic differentiation of the more scattered hBMSC on the scaffolds. Thus, spheres may represent a promising strategy for future TMJ TE.

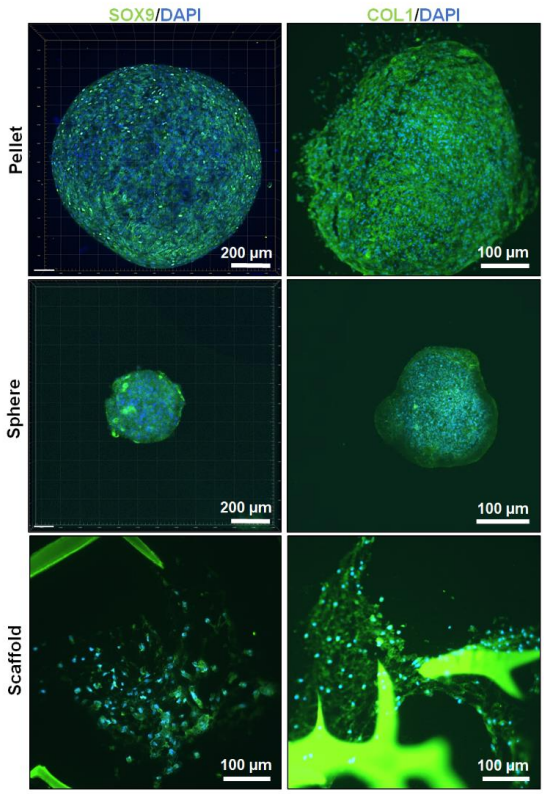

Figure 24. Immunofluorescence staining for SOX9 and COL1 (green signal) in Study III. Nuclei stained with DAPI (blue signal).

In summary, 3D printed scaffolds combined with cell therapy is a promising strategy for customized treatment of degenerative TMJ conditions. The mechanical properties of 3D printed hydrogel scaffolds limit their application to smaller-sized defects. By combining gelatin with a thermoplastic polymer, it can potentially be used for load-bearing applications of the TMJ. Individualized clinical cell therapy is associated with considerable costs. However, the impact of an effective treatment of degenerative joint disease will be significant for the suffering patient's quality of life and the financial burden on society. Hopefully, future joint collaborations between clinicians and researchers can provide a viable treatment options for the vast majority.

6. Conclusions

The current project represents a preliminary exploration of factors of importance in the TE approach of cartilaginous structures of the TMJ. Based on the results, the following conclusions can be drawn:

- Angiostatin reduces the angiogenic and inflammatory response to collagen scaffolds seeded with rBMSC *in vivo,* although this itself does not induce chondrogenesis (Study I).
- The current preclinical evidence indicates superior regeneration of TMJ cartilage tissues by scaffolds seeded with chondrogenic cells, compared to cell-free scaffolds. Differentiation of cells pre-implantation is advantageous (Study II).
- Gelatin demonstrated high suitability for scaffold fabrication via 3D printing (Studies III and IV).
- 3D printed gelatin scaffolds crosslinked with genipin are cytocompatible, support the chondrogenic differentiation and limits the hypertrophic tendency of hBMSC *in vitro* (Study III).
- Dual crosslinking of 3D printed gelatin scaffolds with DHT and ribose enhances the mechanical and degradation properties, and support chondrogenic differentiation of rBMSC *in vitro* (Study IV).
- The mechanical properties of 3D printed gelatin limit its potential application to smaller, non-load bearing defects (Studies III and IV).

7. Future perspectives

The future of 3D printing technology and MSC in TMJ TE seems promising. These technological developments will allow medicine to be tailored toward specific patients. Recently, 3D printed TMJ prostheses with customized design have been introduced in clinical applications [200]. The use of autologous MSC is approved for clinical trials in Europe and their safety and efficacy have been reported for maxillofacial bone regeneration [201]. For clinical trials, safe and approved biomaterials must be used in combination with the MSC. Although gelatin is classified as GRAS by the FDA, a scaffold combining gelatin and MSC requires long and expensive clinical approval procedures. Moreover, the mechanical properties of the 3D printed gelatin scaffolds are not sufficient for load-bearing applications. The use of mechanically stronger and FDA-approved materials such as PCL can facilitate the translation of 3D printing technology to the clinic. However, toward human translation, the safety and efficacy of these tissue engineered TMJ 3D printed scaffolds must be evaluated in a suitable large animal model. Minipigs represents one of the more clinical translational animal models based on their TMJ anatomy and biology [42, 142] and would offer a suitable platform to test new TMJ TE strategies. This requires the development of an appropriate defect model and the surgical techniques to fix the scaffolds into the TMJ. Altogether, the need for further research is necessary to pave the path of TMJ 3D printed scaffolds from bench to bedside.

Based on the results of the current thesis, the future research should include:

- Functionalization of 3D printed gelatin with angiostatin. The dose and controlled release should be further optimized to maximize its effect on MSC.
- Although gelatin demonstrated high 3D printability, the scaffold design should be further optimized with respect to internal architecture and porosity. Co-printing of gelatin hydrogel between strong thermoplastic polymeric filaments such as PCL should be adopted to improve the mechanical properties of the scaffolds.

- The chondrogenic potential of MSC spheres printed in gelatin hydrogel should be further investigated *in vitro* and *in vivo*.
- To facilitate clinical translation, the regenerative potential of 3D printed gelatin scaffolds with MSC should be investigated in orthotopic TMJ models, e.g. disc and/or condyle defects in minipig model.

8. References

1. Scrivani, S.J., D.A. Keith, and L.B. Kaban, *Temporomandibular disorders.* N Engl J Med, 2008. **359**(25): p. 2693-705.
2. Johansson, A., et al., *Gender difference in symptoms related to temporomandibular disorders in a population of 50-year-old subjects.* J Orofac Pain, 2003. **17**(1): p. 29-35.
3. Manfredini, D., et al., *Research diagnostic criteria for temporomandibular disorders: a systematic review of axis I epidemiologic findings.* Oral Surgery, Oral Medicine, Oral Pathology, Oral Radiology, and Endodontology, 2011. **112**(4): p. 453-462.
4. Bueno, C.H., et al., *Gender differences in temporomandibular disorders in adult populational studies: A systematic review and meta-analysis.* Journal of Oral Rehabilitation, 2018. **45**(9): p. 720-729.
5. Alomar, X., et al., *Anatomy of the temporomandibular joint.* Semin Ultrasound CT MR, 2007. **28**(3): p. 170-83.
6. Almarza, A.J. and K.A. Athanasiou, *Design characteristics for the tissue engineering of cartilaginous tissues.* Ann Biomed Eng, 2004. **32**(1): p. 2-17.
7. Lowe, J. and A.J. Almarza, *A review of in-vitro fibrocartilage tissue engineered therapies with a focus on the temporomandibular joint.* Arch Oral Biol, 2017. **83**: p. 193-201.
8. Kuroda, S., et al., *Biomechanical and biochemical characteristics of the mandibular condylar cartilage.* Osteoarthritis Cartilage, 2009. **17**(11): p. 1408-15.
9. Whyte, A.M., et al., *Magnetic resonance imaging in the evaluation of temporomandibular joint disc displacement—a review of 144 cases.* 2006. **35**(8): p. 696-703.
10. Holmlund, A., *Disc derangements of the temporomandibular joint.* International Journal of Oral and Maxillofacial Surgery, 2007. **36**(7): p. 571-576.
11. American Society of Temporomandibular Joint, S., *Guidelines for diagnosis and management of disorders involving the temporomandibular joint and related musculoskeletal structures.* Cranio, 2003. **21**(1): p. 68-76.
12. de Bont, L.G., et al., *Osteoarthritis and internal derangement of the temporomandibular joint: a light microscopic study.* J Oral Maxillofac Surg, 1986. **44**(8): p. 634-43.
13. Paegle, D.I., A.B. Holmlund, and A. Hjerpe, *Matrix glycosaminoglycans in the temporomandibular joint in patients with painful clicking and chronic closed lock.* 2003. **32**(4): p. 397-400.
14. Tan, A.R. and C.T. Hung, *Concise Review: Mesenchymal Stem Cells for Functional Cartilage Tissue Engineering: Taking Cues from Chondrocyte-Based Constructs.* Stem Cells Transl Med, 2017. **6**(4): p. 1295-1303.
15. Chaganti, R.K. and N.E. Lane, *Risk factors for incident osteoarthritis of the hip and knee.* 2011. **4**(3): p. 99-104.
16. Buckwalter, J. and J. Martin, *Osteoarthritis ☆.* Advanced Drug Delivery Reviews, 2006. **58**(2): p. 150-167.
17. Tjakkes, G.H., et al., *TMD pain: the effect on health related quality of life and the influence of pain duration.* Health Qual Life Outcomes, 2010. **8**: p. 46.

18. Kalladka, M., et al., *Temporomandibular joint osteoarthritis: diagnosis and long-term conservative management: a topic review.* J Indian Prosthodont Soc, 2014. **14**(1): p. 6-15.
19. Chen, D., et al., *Osteoarthritis: toward a comprehensive understanding of pathological mechanism.* Bone Research, 2017. **5**: p. 16044.
20. Wang, X.D., et al., *Current Understanding of Pathogenesis and Treatment of TMJ Osteoarthritis.* Journal of Dental Research, 2015. **94**(5): p. 666-673.
21. Pelttari, K., A. Wixmerten, and I. Martin, *Do we really need cartilage tissue engineering?* Swiss Med Wkly, 2009. **139**(41-42): p. 602-9.
22. Dimitroulis, G., *Management of temporomandibular joint disorders: A surgeon's perspective.* Australian Dental Journal, 2018. **63**: p. S79-S90.
23. Widmark, G., *On surgical intervention in the temporomandibular joint.* Swedish dental journal. Supplement, 1997. **123**: p. 1-87.
24. Dolwick, M.F., *Temporomandibular joint surgery for internal derangement.* Dent Clin North Am, 2007. **51**(1): p. 195-208, vii-viii.
25. Holmlund, A., B. Lund, and C.K. Weiner, *Discectomy without replacement for the treatment of painful reciprocal clicking or catching and chronic closed lock of the temporomandibular joint: a clinical follow-up audit.* Br J Oral Maxillofac Surg, 2013. **51**(8): p. e211-4.
26. Dimitroulis, G., *A critical review of interpositional grafts following temporomandibular joint discectomy with an overview of the dermis-fat graft.* Int J Oral Maxillofac Surg, 2011. **40**(6): p. 561-8.
27. Ferreira, J.N., et al., *Evaluation of surgically retrieved temporomandibular joint alloplastic implants: pilot study.* J Oral Maxillofac Surg, 2008. **66**(6): p. 1112-24.
28. Dolwick, M.F. and G. Dimitroulis, *Is there a role for temporomandibular joint surgery?* Br J Oral Maxillofac Surg, 1994. **32**(5): p. 307-13.
29. Gonzalez-Perez, L.M., et al., *Two-year prospective study of outcomes following total temporomandibular joint replacement.* 2016. **45**(1): p. 78-84.
30. Donahue, R.P., J.C. Hu, and K.A. Athanasiou, *Remaining Hurdles for Tissue-Engineering the Temporomandibular Joint Disc.* Trends Mol Med, 2019.
31. Williams, D.F., *To engineer is to create: the link between engineering and regeneration.* 2006. **24**(1): p. 4-8.
32. Jeong, H.J., S.H. Lee, and C.S. Ko, *Meniscectomy.* Knee Surg Relat Res, 2012. **24**(3): p. 129-36.
33. Vacanti, J.P., et al., *Selective cell transplantation using bioabsorbable artificial polymers as matrices.* 1988. **23**(1): p. 3-9.
34. O'Brien, F.J., *Biomaterials & scaffolds for tissue engineering.* Materials Today, 2011. **14**(3): p. 88-95.
35. Huey, D.J., J.C. Hu, and K.A. Athanasiou, *Unlike Bone, Cartilage Regeneration Remains Elusive.* Science, 2012. **338**(6109): p. 917-921.
36. Johnstone, B., et al., *Tissue engineering for articular cartilage repair--the state of the art.* Eur Cell Mater, 2013. **25**: p. 248-67.
37. Cao, Y., et al., *Transplantation of chondrocytes utilizing a polymer-cell construct to produce tissue-engineered cartilage in the shape of a human ear.* Plast Reconstr Surg, 1997. **100**(2): p. 297-302; discussion 303-4.
38. Chen, S., et al., *Strategies to minimize hypertrophy in cartilage engineering and regeneration.* Genes & Diseases, 2015. **2**(1): p. 76-95.
39. Harris, J.D., et al., *Autologous chondrocyte implantation: a systematic review.* J Bone Joint Surg Am, 2010. **92**(12): p. 2220-33.

40. De Souza Tesch, R., et al., *Temporomandibular joint regeneration: proposal of a novel treatment for condylar resorption after orthognathic surgery using transplantation of autologous nasal septum chondrocytes, and the first human case report.* Stem Cell Research & Therapy, 2018. **9**(1).
41. Anderson, D.E. and K.A. Athanasiou, *A comparison of primary and passaged chondrocytes for use in engineering the temporomandibular joint.* Arch Oral Biol, 2009. **54**(2): p. 138-45.
42. Vapniarsky, N., et al., *Tissue engineering toward temporomandibular joint disc regeneration.* Sci Transl Med, 2018. **10**(446).
43. Centola, M., et al., *Scaffold-based delivery of a clinically relevant anti-angiogenic drug promotes the formation of in vivo stable cartilage.* Tissue Eng Part A, 2013. **19**(17-18): p. 1960-71.
44. Liao, H.T., et al., *Prefabricated, ear-shaped cartilage tissue engineering by scaffold-free porcine chondrocyte membrane.* Plast Reconstr Surg, 2015. **135**(2): p. 313e-21e.
45. Embree, M.C., et al., *Exploiting endogenous fibrocartilage stem cells to regenerate cartilage and repair joint injury.* Nat Commun, 2016. **7**: p. 13073.
46. Guterl, C.C., et al., *Characterization of Mechanics and Cytocompatibility of Fibrin-Genipin Annulus Fibrosus Sealant with the Addition of Cell Adhesion Molecules.* 2014. **20**(17-18): p. 2536-2545.
47. Bauge, C. and K. Boumediene, *Use of Adult Stem Cells for Cartilage Tissue Engineering: Current Status and Future Developments.* Stem Cells Int, 2015. **2015**: p. 438026.
48. Friedenstein, A.J., et al., *Heterotopic of bone marrow. Analysis of precursor cells for osteogenic and hematopoietic tissues.* Transplantation, 1968. **6**(2): p. 230-47.
49. Shanti, R.M., et al., *Adult mesenchymal stem cells: biological properties, characteristics, and applications in maxillofacial surgery.* J Oral Maxillofac Surg, 2007. **65**(8): p. 1640-7.
50. Pittenger, M.F., et al., *Multilineage potential of adult human mesenchymal stem cells.* Science, 1999. **284**(5411): p. 143-7.
51. Dominici, M., et al., *Minimal criteria for defining multipotent mesenchymal stromal cells. The International Society for Cellular Therapy position statement.* Cytotherapy, 2006. **8**(4): p. 315-7.
52. Beane, O.S. and E.M. Darling, *Isolation, characterization, and differentiation of stem cells for cartilage regeneration.* Ann Biomed Eng, 2012. **40**(10): p. 2079-97.
53. Mehlhorn, A.T., et al., *Differential expression pattern of extracellular matrix molecules during chondrogenesis of mesenchymal stem cells from bone marrow and adipose tissue.* Tissue Eng, 2006. **12**(10): p. 2853-62.
54. Mohamed-Ahmed, S., et al., *Adipose-derived and bone marrow mesenchymal stem cells: a donor-matched comparison.* Stem Cell Res Ther, 2018. **9**(1): p. 168.
55. Kim, M., et al., *Donor Variation and Optimization of Human Mesenchymal Stem Cell Chondrogenesis in Hyaluronic Acid.* Tissue Eng Part A, 2018. **24**(21-22): p. 1693-1703.
56. Wang, Y., et al., *Plasticity of mesenchymal stem cells in immunomodulation: pathological and therapeutic implications.* 2014. **15**(11): p. 1009-1016.
57. Caplan, A.I., *Mesenchymal Stem Cells: Time to Change the Name!* STEM CELLS Translational Medicine, 2017. **6**(6): p. 1445-1451.
58. De Windt, T.S., et al., *Allogeneic Mesenchymal Stem Cells Stimulate Cartilage Regeneration and Are Safe for Single-Stage Cartilage Repair in Humans upon Mixture with Recycled Autologous Chondrons.* STEM CELLS, 2017. **35**(1): p. 256-264.

59. Caplan, A.I. and D. Correa, *The MSC: an injury drugstore.* Cell Stem Cell, 2011. **9**(1): p. 11-5.
60. Li, J. and S. Dong, *The Signaling Pathways Involved in Chondrocyte Differentiation and Hypertrophic Differentiation.* Stem Cells International, 2016. **2016**: p. 1-12.
61. Kozhemyakina, E., A.B. Lassar, and E. Zelzer, *A pathway to bone: signaling molecules and transcription factors involved in chondrocyte development and maturation.* Development, 2015. **142**(5): p. 817-831.
62. Lefebvre, V. and M. Dvir-Ginzberg, *SOX9 and the many facets of its regulation in the chondrocyte lineage.* Connect Tissue Res, 2017. **58**(1): p. 2-14.
63. Staffler, A., et al., *Heterozygous SOX9 Mutations Allowing for Residual DNA-binding and Transcriptional Activation Lead to the Acampomelic Variant of Campomelic Dysplasia.* 2010. **31**(6): p. E1436-E1444.
64. Sekiya, I., et al., *SOX9 enhances aggrecan gene promoter/enhancer activity and is up-regulated by retinoic acid in a cartilage-derived cell line, TC6.* J Biol Chem, 2000. **275**(15): p. 10738-44.
65. Ng, L.J., et al., *SOX9 binds DNA, activates transcription, and coexpresses with type II collagen during chondrogenesis in the mouse.* Dev Biol, 1997. **183**(1): p. 108-21.
66. Kiani, C., et al., *Structure and function of aggrecan.* Cell Research, 2002. **12**(1): p. 19-32.
67. Johnstone, B., et al., *In vitro chondrogenesis of bone marrow-derived mesenchymal progenitor cells.* Exp Cell Res, 1998. **238**(1): p. 265-72.
68. Rogan, H., F. Ilagan, and F. Yang, *Comparing Single Cell vs. Pellet Encapsulation of MSCs in 3D Hydrogels for Cartilage Regeneration.* Tissue Engineering Part A, 2019.
69. Solchaga, L.A., K.J. Penick, and J.F. Welter, *Chondrogenic Differentiation of Bone Marrow-Derived Mesenchymal Stem Cells: Tips and Tricks*. 2011, Humana Press. p. 253-278.
70. Tare, R.S., et al., *Tissue engineering strategies for cartilage generation—Micromass and three dimensional cultures using human chondrocytes and a continuous cell line.* Biochemical and Biophysical Research Communications, 2005. **333**(2): p. 609-621.
71. Sart, S., et al., *Three-Dimensional Aggregates of Mesenchymal Stem Cells: Cellular Mechanisms, Biological Properties, and Applications.* Tissue Engineering Part B: Reviews, 2014. **20**(5): p. 365-380.
72. Moll, G., et al., *Are Therapeutic Human Mesenchymal Stromal Cells Compatible with Human Blood?* 2012. **30**(7): p. 1565-1574.
73. Cesarz, Z. and K. Tamama, *Spheroid Culture of Mesenchymal Stem Cells.* Stem Cells Int, 2016. **2016**: p. 9176357.
74. Vallier, L. and R.A. Pedersen, *Human Embryonic Stem Cells: An In Vitro Model to Study Mechanisms Controlling Pluripotency in Early Mammalian Development.* 2005. **1**(2): p. 119-130.
75. Hildebrandt, C., H. Büth, and H. Thielecke, *A scaffold-free in vitro model for osteogenesis of human mesenchymal stem cells.* 2011. **43**(2): p. 91-100.
76. Baraniak, P.R. and T.C. McDevitt, *Scaffold-free culture of mesenchymal stem cell spheroids in suspension preserves multilineage potential.* 2012. **347**(3): p. 701-711.
77. Futrega, K., et al., *The microwell-mesh: A novel device and protocol for the high throughput manufacturing of cartilage microtissues.* 2015. **62**: p. 1-12.
78. Acharya, C., et al., *Enhanced chondrocyte proliferation and mesenchymal stromal cells chondrogenesis in coculture pellets mediate improved cartilage formation.* 2012. **227**(1): p. 88-97.

79. Jones, B.A. and M. Pei, *Synovium-derived stem cells: a tissue-specific stem cell for cartilage engineering and regeneration.* Tissue Eng Part B Rev, 2012. **18**(4): p. 301-11.
80. Sun, X.D., et al., *Non-viral endostatin plasmid transfection of mesenchymal stem cells via collagen scaffolds.* Biomaterials, 2009. **30**(6): p. 1222-31.
81. Jeng, L., B.R. Olsen, and M. Spector, *Engineering endostatin-producing cartilaginous constructs for cartilage repair using nonviral transfection of chondrocyte-seeded and mesenchymal-stem-cell-seeded collagen scaffolds.* Tissue Eng Part A, 2010. **16**(10): p. 3011-21.
82. Lee, J., M.J. Cuddihy, and N.A. Kotov, *Three-Dimensional Cell Culture Matrices: State of the Art.* 2008. **14**(1): p. 61-86.
83. Hu, J.C. and K.A. Athanasiou, *A self-assembling process in articular cartilage tissue engineering.* Tissue Eng, 2006. **12**(4): p. 969-79.
84. Rai, V., et al., *Recent strategies in cartilage repair: A systemic review of the scaffold development and tissue engineering.* Journal of Biomedical Materials Research Part A, 2017. **105**(8): p. 2343-2354.
85. Francis, S.L., et al., *Cartilage Tissue Engineering Using Stem Cells and Bioprinting Technology—Barriers to Clinical Translation.* Frontiers in Surgery, 2018. **5**(70).
86. Cao, Z., C. Dou, and S. Dong, *Scaffolding Biomaterials for Cartilage Regeneration.* 2014. **2014**: p. 1-8.
87. Tarafder, S., et al., *Micro-precise spatiotemporal delivery system embedded in 3D printing for complex tissue regeneration.* Biofabrication, 2016. **8**(2): p. 025003.
88. Ahtiainen, K., et al., *Autologous adipose stem cells and polylactide discs in the replacement of the rabbit temporomandibular joint disc.* J R Soc Interface, 2013. **10**(85): p. 20130287.
89. Liu, D., et al., *Collagen and Gelatin.* Annual Review of Food Science and Technology, 2015. **6**(1): p. 527-557.
90. Higuchi, A., et al., *Biomimetic Cell Culture Proteins as Extracellular Matrices for Stem Cell Differentiation.* 2012. **112**(8): p. 4507-4540.
91. Irawan, V., et al., *Collagen Scaffolds in Cartilage Tissue Engineering and Relevant Approaches for Future Development.* Tissue Eng Regen Med, 2018. **15**(6): p. 673-697.
92. Su, K. and C. Wang, *Recent advances in the use of gelatin in biomedical research.* Biotechnol Lett, 2015. **37**(11): p. 2139-45.
93. Santoro, M., A.M. Tatara, and A.G. Mikos, *Gelatin carriers for drug and cell delivery in tissue engineering.* Journal of Controlled Release, 2014. **190**: p. 210-218.
94. Echave, M.C., et al., *Gelatin as Biomaterial for Tissue Engineering.* Curr Pharm Des, 2017. **23**(24): p. 3567-3584.
95. Tan, T.C., A.F. AlKarkhi, and A.M. Easa, *Assessment of the ribose-induced Maillard reaction as a means of gelatine powder identification and quality control.* Food Chem, 2012. **134**(4): p. 2430-6.
96. Elzoghby, A.O., W.M. Samy, and N.A. Elgindy, *Protein-based nanocarriers as promising drug and gene delivery systems.* J Control Release, 2012. **161**(1): p. 38-49.
97. Gorgieva, S. and V. Kokol, *Collagen- vs. Gelatine-Based Biomaterials and Their Biocompatibility: Review and Perspectives*. 2011, InTech.
98. Cortesi, R., C. Nastruzzi, and S.S. Davis, *Sugar cross-linked gelatin for controlled release: microspheres and disks.* Biomaterials, 1998. **19**(18): p. 1641-9.
99. Oryan, A., et al., *Chemical crosslinking of biopolymeric scaffolds: Current knowledge and future directions of crosslinked engineered bone scaffolds.* Int J Biol Macromol, 2018. **107**(Pt A): p. 678-688.

100. Ciardelli, G., et al., *Enzymatically crosslinked porous composite matrices for bone tissue regeneration.* 2010. **92A**(1): p. 137-151.
101. Ma, B., et al., *Crosslinking strategies for preparation of extracellular matrix-derived cardiovascular scaffolds.* 2014. **1**(1): p. 81-89.
102. Wang, C., et al., *Cytocompatibility study of a natural biomaterial crosslinker-Genipin with therapeutic model cells.* 2011. **97B**(1): p. 58-65.
103. Cheng, N.C., et al., *Genipin-crosslinked cartilage-derived matrix as a scaffold for human adipose-derived stem cell chondrogenesis.* Tissue Eng Part A, 2013. **19**(3-4): p. 484-96.
104. Sell, S.A., et al., *Cross-linking methods of electrospun fibrinogen scaffolds for tissue engineering applications.* 2008. **3**(4): p. 045001.
105. Silva, S.S., et al., *Novel Genipin-Cross-Linked Chitosan/Silk Fibroin Sponges for Cartilage Engineering Strategies.* 2008. **9**(10): p. 2764-2774.
106. Zhang, X., et al., *The effects of different crossing-linking conditions of genipin on type I collagen scaffolds: an in vitro evaluation.* 2014. **15**(4): p. 531-541.
107. Tanaka, S., et al., *Isolation and partial characterization of collagen chains dimerized by sugar-derived cross-links.* J Biol Chem, 1988. **263**(33): p. 17650-7.
108. Shankar, K.G., et al., *Investigation of different cross-linking approaches on 3D gelatin scaffolds for tissue engineering application: A comparative analysis.* Int J Biol Macromol, 2017. **95**: p. 1199-1209.
109. Krishnakumar, G.S., et al., *Importance of crosslinking strategies in designing smart biomaterials for bone tissue engineering: A systematic review.* Mater Sci Eng C Mater Biol Appl, 2019. **96**: p. 941-954.
110. Turnbull, G., et al., *3D bioactive composite scaffolds for bone tissue engineering.* Bioactive Materials, 2018. **3**(3): p. 278-314.
111. Bandyopadhyay, A., S. Bose, and S. Das, *3D printing of biomaterials.* MRS Bulletin, 2015. **40**(2): p. 108-115.
112. Cibelli, J., et al., *Strategies for improving animal models for regenerative medicine.* Cell Stem Cell, 2013. **12**(3): p. 271-4.
113. Gomes, P.S. and M.H. Fernandes, *Rodent models in bone-related research: the relevance of calvarial defects in the assessment of bone regeneration strategies.* Lab Anim, 2011. **45**(1): p. 14-24.
114. Almarza, A.J., et al., *Preclinical Animal Models for Temporomandibular Joint Tissue Engineering.* Tissue Engineering Part B: Reviews, 2018. **24**(3): p. 171-178.
115. Maniatopoulos, C., J. Sodek, and A.H. Melcher, *Bone formation in vitro by stromal cells obtained from bone marrow of young adult rats.* Cell Tissue Res, 1988. **254**(2): p. 317-30.
116. Schwarz, F., G. Iglhaut, and J. Becker, *Quality assessment of reporting of animal studies on pathogenesis and treatment of peri-implant mucositis and peri-implantitis. A systematic review using the ARRIVE guidelines.* J Clin Periodontol, 2012. **39 Suppl 12**: p. 63-72.
117. Hooijmans, C.R., et al., *Meta-analyses of animal studies: an introduction of a valuable instrument to further improve healthcare.* ILAR J, 2014. **55**(3): p. 418-26.
118. Gostynska, N., et al., *3D porous collagen scaffolds reinforced by glycation with ribose for tissue engineering application.* Biomed Mater, 2017. **12**(5): p. 055002.
119. Balakrishnan, B. and A. Jayakrishnan, *Self-cross-linking biopolymers as injectable in situ forming biodegradable scaffolds.* Biomaterials, 2005. **26**(18): p. 3941-3951.
120. Zhang, Y., T. Pizzute, and M. Pei, *Anti-inflammatory strategies in cartilage repair.* Tissue Eng Part B Rev, 2014. **20**(6): p. 655-68.

121. Benjamin, M. and J.R. Ralphs, *Fibrocartilage in tendons and ligaments--an adaptation to compressive load.* J Anat, 1998. **193 (Pt 4)**: p. 481-94.
122. Carlevaro, M.F., et al., *Vascular endothelial growth factor (VEGF) in cartilage neovascularization and chondrocyte differentiation: auto-paracrine role during endochondral bone formation.* J Cell Sci, 2000. **113 (Pt 1)**: p. 59-69.
123. Athanasiou, K.A., et al., *Self-Organization and the Self-Assembling Process in Tissue Engineering.* Annual Review of Biomedical Engineering, 2013. **15**(1): p. 115-136.
124. Brittberg, M., et al., *Treatment of Deep Cartilage Defects in the Knee with Autologous Chondrocyte Transplantation.* New England Journal of Medicine, 1994. **331**(14): p. 889-895.
125. Naujoks, C., et al., *Principles of cartilage tissue engineering in TMJ reconstruction.* Head Face Med, 2008. **4**: p. 3.
126. Nagao, M., et al., *Vascular Endothelial Growth Factor in Cartilage Development and Osteoarthritis.* Sci Rep, 2017. **7**(1): p. 13027.
127. Kumagai, K., et al., *The levels of vascular endothelial growth factor in the synovial fluid correlated with the severity of arthroscopically observed synovitis and clinical outcome after temporomandibular joint irrigation in patients with chronic closed lock.* Oral Surg Oral Med Oral Pathol Oral Radiol Endod, 2010. **109**(2): p. 185-90.
128. Hamilton, J.L., et al., *Targeting VEGF and Its Receptors for the Treatment of Osteoarthritis and Associated Pain.* J Bone Miner Res, 2016. **31**(5): p. 911-24.
129. Kardel, R., et al., *Inflammatory cell and cytokine patterns in patients with painful clicking and osteoarthritis in the temporomandibular joint.* Int J Oral Maxillofac Surg, 2003. **32**(4): p. 390-6.
130. Jiang, X., et al., *The role of Sox9 in collagen hydrogel-mediated chondrogenic differentiation of adult mesenchymal stem cells (MSCs).* Biomaterials Science, 2018. **6**(6): p. 1556-1568.
131. Wagner, T., et al., *Autosomal sex reversal and campomelic dysplasia are caused by mutations in and around the SRY-related gene SOX9.* Cell, 1994. **79**(6): p. 1111-1120.
132. Murakami, S., V. Lefebvre, and B. de Crombrugghe, *Potent inhibition of the master chondrogenic factor Sox9 gene by interleukin-1 and tumor necrosis factor-alpha.* J Biol Chem, 2000. **275**(5): p. 3687-92.
133. Sheikh, Z., et al., *Macrophages, Foreign Body Giant Cells and Their Response to Implantable Biomaterials.* Materials (Basel), 2015. **8**(9): p. 5671-5701.
134. Scott, M.A., et al., *Brief review of models of ectopic bone formation.* Stem Cells Dev, 2012. **21**(5): p. 655-67.
135. Bornes, T.D., et al., *Optimal Seeding Densities for In Vitro Chondrogenesis of Two- and Three-Dimensional-Isolated and -Expanded Bone Marrow-Derived Mesenchymal Stromal Stem Cells Within a Porous Collagen Scaffold.* Tissue Eng Part C Methods, 2016. **22**(3): p. 208-20.
136. De Vries, R.B.M., et al., *The Usefulness of Systematic Reviews of Animal Experiments for the Design of Preclinical and Clinical Studies.* ILAR Journal, 2014. **55**(3): p. 427-437.
137. Stavropoulos, A., et al., *Pre-clinical in vivo models for the screening of bone biomaterials for oral/craniofacial indications: focus on small-animal models.* Periodontol 2000, 2015. **68**(1): p. 55-65.
138. Herring, S.W., *TMJ anatomy and animal models.* J Musculoskelet Neuronal Interact, 2003. **3**(4): p. 391-4; discussion 406-7.
139. Little, C.B. and M.M. Smith, *Animal models of osteoarthritis.* Current Rheumatology Reviews, 2008. **4**(3): p. 175-182.

140. Hakim, M.A., et al., *In vivo investigation of temporomandibular joint regeneration: development of a mouse model.* International Journal of Oral and Maxillofacial Surgery, 2020.
141. Cook, J.L., et al., *Animal models of cartilage repair.* Bone Joint Res, 2014. **3**(4): p. 89-94.
142. Vapniarsky, N., et al., *The Yucatan minipig TMJ disc structure-function relationships support its suitability for human comparative studies.* Tissue Eng Part C Methods, 2017.
143. Murphy, M.K., et al., *Engineering a fibrocartilage spectrum through modulation of aggregate redifferentiation.* Cell Transplant, 2015. **24**(2): p. 235-45.
144. Schek, R.M., et al., *Tissue engineering osteochondral implants for temporomandibular joint repair.* Orthod Craniofac Res, 2005. **8**(4): p. 313-9.
145. Puelacher, W.C., et al., *Temporomandibular joint disc replacement made by tissue-engineered growth of cartilage.* J Oral Maxillofac Surg, 1994. **52**(11): p. 1172-7; discussion 1177-8.
146. Han, C., J. Li, and C. Hu, *[Reconstruction of TMJ condyle cartilage defects with autogenous free periosteal grafts].* Zhonghua Kou Qiang Yi Xue Za Zhi, 1996. **31**(1): p. 42-4.
147. Yao, X., X. Ma, and Z. Zhang, *[The repairment of the condylar cartilage defect by transplantation of chondrocytes embedded in the collagen membrane].* Zhonghua Kou Qiang Yi Xue Za Zhi, 2000. **35**(2): p. 138-41.
148. Weng, Y., et al., *Tissue-engineered composites of bone and cartilage for mandible condylar reconstruction.* J Oral Maxillofac Surg, 2001. **59**(2): p. 185-90.
149. Suzuki, T., et al., *Regeneration of defects in the articular cartilage in rabbit temporomandibular joints by bone morphogenetic protein-2.* Br J Oral Maxillofac Surg, 2002. **40**(3): p. 201-6.
150. Chen, F., et al., *Bone graft in the shape of human mandibular condyle reconstruction via seeding marrow-derived osteoblasts into porous coral in a nude mice model.* J Oral Maxillofac Surg, 2002. **60**(10): p. 1155-9.
151. Ueki, K., et al., *The use of polylactic acid/polyglycolic acid copolymer and gelatin sponge complex containing human recombinant bone morphogenetic protein-2 following condylectomy in rabbits.* J Craniomaxillofac Surg, 2003. **31**(2): p. 107-14.
152. Alhadlaq, A. and J.J. Mao, *Tissue-engineered neogenesis of human-shaped mandibular condyle from rat mesenchymal stem cells.* J Dent Res, 2003. **82**(12): p. 951-6.
153. Chan, W.P., et al., *MRI and histology of collagen template disc implantation and regeneration in rabbit temporomandibular joint: preliminary report.* Transplant Proc, 2004. **36**(5): p. 1610-2.
154. Lai, W.F., et al., *Histological analysis of regeneration of temporomandibular joint discs in rabbits by using a reconstituted collagen template.* Int J Oral Maxillofac Surg, 2005. **34**(3): p. 311-20.
155. Alhadlaq, A. and J.J. Mao, *Tissue-engineered osteochondral constructs in the shape of an articular condyle.* J Bone Joint Surg Am, 2005. **87**(5): p. 936-44.
156. Takafuji, H., et al., *Regeneration of articular cartilage defects in the temporomandibular joint of rabbits by fibroblast growth factor-2: a pilot study.* Int J Oral Maxillofac Surg, 2007. **36**(10): p. 934-7.
157. El-Bialy, T., et al., *In vivo ultrasound-assisted tissue-engineered mandibular condyle: a pilot study in rabbits.* Tissue Eng Part C Methods, 2010. **16**(6): p. 1315-23.

158. Yu, H., et al., *Distraction osteogenesis combined with tissue-engineered cartilage in the reconstruction of condylar osteochondral defect.* J Oral Maxillofac Surg, 2011. **69**(12): p. e558-64.
159. Zhu, S., et al., *NEL-like molecule-1-modified bone marrow mesenchymal stem cells/poly lactic-co-glycolic acid composite improves repair of large osteochondral defects in mandibular condyle.* Osteoarthritis Cartilage, 2011. **19**(6): p. 743-50.
160. Dormer, N.H., et al., *Osteochondral interface regeneration of rabbit mandibular condyle with bioactive signal gradients.* J Oral Maxillofac Surg, 2011. **69**(6): p. e50-7.
161. Zheng, Y.H., et al., *Basic fibroblast growth factor enhances osteogenic and chondrogenic differentiation of human bone marrow mesenchymal stem cells in coral scaffold constructs.* J Tissue Eng Regen Med, 2011. **5**(7): p. 540-50.
162. Brown, B.N., et al., *Extracellular matrix as an inductive template for temporomandibular joint meniscus reconstruction: a pilot study.* J Oral Maxillofac Surg, 2011. **69**(12): p. e488-505.
163. Zheng, Y.H., et al., *[New bone and cartilage tissues formed from human bone marrow mesenchymal stem cells derived from human condyle in vivo].* Zhonghua Kou Qiang Yi Xue Za Zhi, 2012. **47**(1): p. 10-3.
164. Brown, B.N., et al., *Inductive, scaffold-based, regenerative medicine approach to reconstruction of the temporomandibular joint disk.* J Oral Maxillofac Surg, 2012. **70**(11): p. 2656-68.
165. Ciocca, L., et al., *Mesenchymal stem cells and platelet gel improve bone deposition within CAD-CAM custom-made ceramic HA scaffolds for condyle substitution.* Biomed Res Int, 2013. **2013**: p. 549762.
166. Li, Y., et al., *Triple-layered cell sheet for tissue-engineering the synovial membrane of the temporomandibular joint.* Cells Tissues Organs, 2014. **199**(2-3): p. 150-8.
167. Wu, Y., et al., *The pilot study of fibrin with temporomandibular joint derived synovial stem cells in repairing TMJ disc perforation.* Biomed Res Int, 2014. **2014**: p. 454021.
168. Kobayashi, E., et al., *Experimental Study on In Situ Tissue Engineering of the Temporomandibular Joint Disc using Autologous Bone Marrow and Collagen Sponge Scaffold.* Journal of Hard Tissue Biology, 2015. **24**(2): p. 211-218.
169. Wang, F., et al., *Regeneration of subcutaneous tissue-engineered mandibular condyle in nude mice.* J Craniomaxillofac Surg, 2017. **45**(6): p. 855-861.
170. Wang, K.H., et al., *Histological and Immunohistochemical Analyses of Repair of the Disc in the Rabbit Temporomandibular Joint Using a Collagen Template.* Materials (Basel), 2017. **10**(8).
171. Amadori, S., et al., *Highly Porous Gelatin Reinforced 3D Scaffolds for Articular Cartilage Regeneration.* 2015. **15**(7): p. 941-952.
172. Contessi Negrini, N., et al., *Three-dimensional printing of chemically crosslinked gelatin hydrogels for adipose tissue engineering.* Biofabrication, 2020. **12**(2): p. 025001.
173. Lewis, P.L., R.M. Green, and R.N. Shah, *3D-printed gelatin scaffolds of differing pore geometry modulate hepatocyte function and gene expression.* Acta Biomater, 2018. **69**: p. 63-70.
174. Levato, R., et al., *The bio in the ink: cartilage regeneration with bioprintable hydrogels and articular cartilage-derived progenitor cells.* Acta Biomaterialia, 2017. **61**: p. 41-53.
175. Jaipan, P., A. Nguyen, and R.J. Narayan, *Gelatin-based hydrogels for biomedical applications.* MRS Communications, 2017. **7**(3): p. 416-426.

176. Li, J., et al., *3D printing of hydrogels: Rational design strategies and emerging biomedical applications.* Materials Science and Engineering: R: Reports, 2020. **140**: p. 100543.
177. Schuurman, W., et al., *Gelatin-Methacrylamide Hydrogels as Potential Biomaterials for Fabrication of Tissue-Engineered Cartilage Constructs.* Macromolecular Bioscience, 2013. **13**(5): p. 551-561.
178. He, Y., et al., *Research on the printability of hydrogels in 3D bioprinting.* Sci Rep, 2016. **6**: p. 29977.
179. Parker, A. and V. Normand, *Glassy dynamics of gelatin gels.* 2010. **6**(19): p. 4916.
180. Yang, G., et al., *Assessment of the characteristics and biocompatibility of gelatin sponge scaffolds prepared by various crosslinking methods.* Sci Rep, 2018. **8**(1): p. 1616.
181. Sung, H.W., et al., *In vitro evaluation of cytotoxicity of a naturally occurring cross-linking reagent for biological tissue fixation.* J Biomater Sci Polym Ed, 1999. **10**(1): p. 63-78.
182. Yang, G., et al., *Assessment of the characteristics and biocompatibility of gelatin sponge scaffolds prepared by various crosslinking methods.* Scientific Reports, 2018. **8**(1).
183. Solorio, L., et al., *Gelatin microspheres crosslinked with genipin for local delivery of growth factors.* Journal of Tissue Engineering and Regenerative Medicine, 2010. **4**(7): p. 514-523.
184. De Clercq, K., et al., *Genipin-crosslinked gelatin microspheres as a strategy to prevent postsurgical peritoneal adhesions: In vitro and in vivo characterization.* Biomaterials, 2016. **96**: p. 33-46.
185. Liang, H.-C., et al., *Crosslinking structures of gelatin hydrogels crosslinked with genipin or a water-soluble carbodiimide.* Journal of Applied Polymer Science, 2004. **91**(6): p. 4017-4026.
186. Khadidja, L., et al., *Alginate/gelatin crosslinked system through Maillard reaction: preparation, characterization and biological properties.* Polymer Bulletin, 2017. **74**(12): p. 4899-4919.
187. Stevenson, M., et al., *Development and characterization of ribose-crosslinked gelatin products prepared by indirect 3D printing.* Food Hydrocolloids, 2019. **96**: p. 65-71.
188. Tanaka, E., et al., *Mechanical properties of human articular disk and its influence on TMJ loading studied with the finite element method.* 2001. **28**(3): p. 273-279.
189. Agata, H., *Isolation of Bone Marrow Stromal Cells: Cellular Composition is Technique-Dependent*. 2013, InTech.
190. Sarem, M., et al., *Cell number in mesenchymal stem cell aggregates dictates cell stiffness and chondrogenesis.* Stem Cell Research & Therapy, 2019. **10**(1).
191. Delise, A.M. and R.S. Tuan, *Analysis of N-cadherin function in limb mesenchymal chondrogenesis in vitro.* Developmental Dynamics, 2002. **225**(2): p. 195-204.
192. Chang, W.-H., et al., *A genipin-crosslinked gelatin membrane as wound-dressing material: in vitro and in vivo studies.* Journal of Biomaterials Science, Polymer Edition, 2003. **14**(5): p. 481-495.
193. Wang, C., et al., *Cytocompatibility study of a natural biomaterial crosslinker-Genipin with therapeutic model cells.* Journal of Biomedical Materials Research Part B: Applied Biomaterials, 2011. **97B**(1): p. 58-65.
194. Olivares, A.L. and D. Lacroix, *Simulation of Cell Seeding Within a Three-Dimensional Porous Scaffold: A Fluid-Particle Analysis.* Tissue Engineering Part C: Methods, 2012. **18**(8): p. 624-631.

195. Declercq, H.A., et al., *Synergistic effect of surface modification and scaffold design of bioplotted 3-D poly-ε-caprolactone scaffolds in osteogenic tissue engineering.* 2013. **9**(8): p. 7699-7708.
196. Chen, S., et al., *Gelatin Scaffolds with Controlled Pore Structure and Mechanical Property for Cartilage Tissue Engineering.* Tissue Eng Part C Methods, 2016. **22**(3): p. 189-98.
197. Han, H.-W., S. Asano, and S.-H. Hsu, *Cellular Spheroids of Mesenchymal Stem Cells and Their Perspectives in Future Healthcare.* Applied Sciences, 2019. **9**(4): p. 627.
198. Yoon, H.H., et al., *Enhanced Cartilage Formation via Three-Dimensional Cell Engineering of Human Adipose-Derived Stem Cells.* 2012. **18**(19-20): p. 1949-1956.
199. Shen, G., *The role of type X collagen in facilitating and regulating endochondral ossification of articular cartilage.* Orthodontics and Craniofacial Research, 2005. **8**(1): p. 11-17.
200. Zheng, J., et al., *An innovative total temporomandibular joint prosthesis with customized design and 3D printing additive fabrication: a prospective clinical study.* Journal of Translational Medicine, 2019. **17**(1).
201. Gjerde, C., et al., *Cell therapy induced regeneration of severely atrophied mandibular bone in a clinical trial.* Stem Cell Research & Therapy, 2018. **9**(1).

9. Original papers

I

Paper I

Angiostatin-functionalized collagen scaffolds suppress angiogenesis but do not induce chondrogenesis by mesenchymal stromal cells *in vivo*

Espen Helgeland, Torbjørn O. Pedersen, Ahmad Rashad, Anne C. Johannessen, Kamal Mustafa, and Annika Rosén

Journal of Oral Science 2020, doi: 10.2334/josnusd.19-0327
[Online ahead of print].

Paper II

II

Scaffold-Based Temporomandibular Joint Tissue Regeneration in Experimental Animal Models: A Systematic Review

Espen Helgeland, Siddharth Shanbhag, Torbjørn O. Pedersen, Kamal Mustafa, and Annika Rosén

Tissue Engineering Part B Rev. 2018, 4, 300-316.

Paper III

III

3D Printed Gelatin-Genipin Scaffolds for Temporomandibular Joint Cartilage Regeneration

Espen Helgeland, Samih Mohamed-Ahmed, Siddharth Shanbhag, Torbjørn O. Pedersen, Annika Rosén, Kamal Mustafa and Ahmad Rashad

Submitted manuscript.

Paper IV

Dual-crosslinked 3D printed gelatin scaffolds with potential for temporomandibular joint cartilage regeneration

Espen Helgeland, Ahmad Rashad, Elisabetta Campodoni, Torbjørn Ostvik Pedersen, Monica Sandri, Annika Rosén and Kamal Mustafa

Submitted manuscript.

IV

Graphic design: Communication Division, UiB / Print: Skipnes Kommunikasjon AS

uib.no

ISBN: 9788230840047 (print)
9788230846704 (PDF)